Cell

Precise Developmental Gene Expression Arises from Globally Stochastic Transcriptional Activity

Shawn C. Little,[1,4] Mikhail Tikhonov,[2,3,4] and Thomas Gregor[2,3,*]
[1]Department of Molecular Biology, Howard Hughes Medical Institute
[2]Joseph Henry Laboratories of Physics
[3]Lewis-Sigler Institute for Integrative Genomics
Princeton University, Princeton, NJ 08544, USA
[4]These authors contributed equally to this work
*Correspondence: tg2@princeton.edu
http://dx.doi.org/10.1016/j.cell.2013.07.025

SUMMARY

Early embryonic patterning events are strikingly precise, a fact that appears incompatible with the stochastic gene expression observed across phyla. Using single-molecule mRNA quantification in *Drosophila* embryos, we determine the magnitude of fluctuations in the expression of four critical patterning genes. The accumulation of mRNAs is identical across genes and fluctuates by only ~8% between neighboring nuclei, generating precise protein distributions. In contrast, transcribing loci exhibit an intrinsic noise of ~45% independent of specific promoter-enhancer architecture or fluctuating inputs. Precise transcript distribution in the syncytium is recovered via straightforward spatiotemporal averaging, i.e., accumulation and diffusion of transcripts during nuclear cycles, without regulatory feedback. Common expression characteristics shared between genes suggest that fluctuations in mRNA production are context independent and are a fundamental property of transcription. The findings shed light on how the apparent paradox between stochastic transcription and developmental precision is resolved.

INTRODUCTION

A fundamental question in biology concerns the degree of precision that cellular systems exhibit in their responses to a given set of environmental conditions, extracellular signals, or other input stimuli (Lagha et al., 2012; Lander 2013, Little and Wieschaus, 2011). Production of and interactions between molecules are intrinsically stochastic, limiting the ability of cells to control gene expression and biochemical activities (Raser and O'Shea, 2005), but the propensity of cellular systems to achieve appropriate phenotypic behavior constrains the tolerable magnitude of molecular fluctuations (Rao et al., 2002). In most contexts, it is unknown how closely cellular activity and phenotypic behavior rely on precise control of gene expression.

Many features of *Drosophila* embryogenesis suggest that strict control of gene expression determines reproducible and precise cell fate establishment. In *Drosophila* embryos, patterned gene expression in the early syncytium of ~6,000 nuclei is triggered by asymmetrically distributed, maternally supplied cues (Sauer et al., 1996). Among these is the transcription factor Bicoid (Bcd), the anterior-posterior (AP) concentration gradient of which shows remarkably reproducible distributions between embryos (Gregor et al., 2007). Moreover, within an embryo, the nuclei at similar AP coordinates differ in Bcd concentration by less than 10% (SD over mean), a degree of precision sufficiently high for each row of cells along the AP axis to discern its position from its immediate neighbors (Gregor et al., 2007). Bcd precision correlates with highly precise protein distribution of zygotically expressed target genes (Dubuis et al., 2013; Gregor et al., 2007) that confer cells with distinct gene expression programs within under 3 hr following fertilization (Gergen et al., 1986; Kornberg and Tabata, 1993).

These observations suggest a model in which tightly regulated transcriptional inputs give rise to rapidly established, highly precise outputs. However, the degree of precision in developmental transcription is largely unexplored. In all contexts assayed from prokaryotes to mammalian cells, absolute levels of a given transcript differ by at least ~50% between genotypically identical cells, and for a majority of genes, this variability is even higher (Cohen et al., 2009; Gandhi et al., 2011; Golding et al., 2005; Paré et al., 2009; Taniguchi et al., 2010; Raj et al., 2006, 2010; Reiter et al., 2011; Sigal et al., 2006; Zenklusen et al., 2008). Quantitative observations support the idea that the process of transcription is intrinsically stochastic (Kaern et al., 2005; Li and Xie, 2011). In developmental contexts, it is unknown whether relatively small input transcription factor fluctuations impact the transcriptional output and whether embryogenesis requires the activity of specialized filtering and/or feedback mechanisms to ensure fidelity in the rapid establishment of gene expression programs.

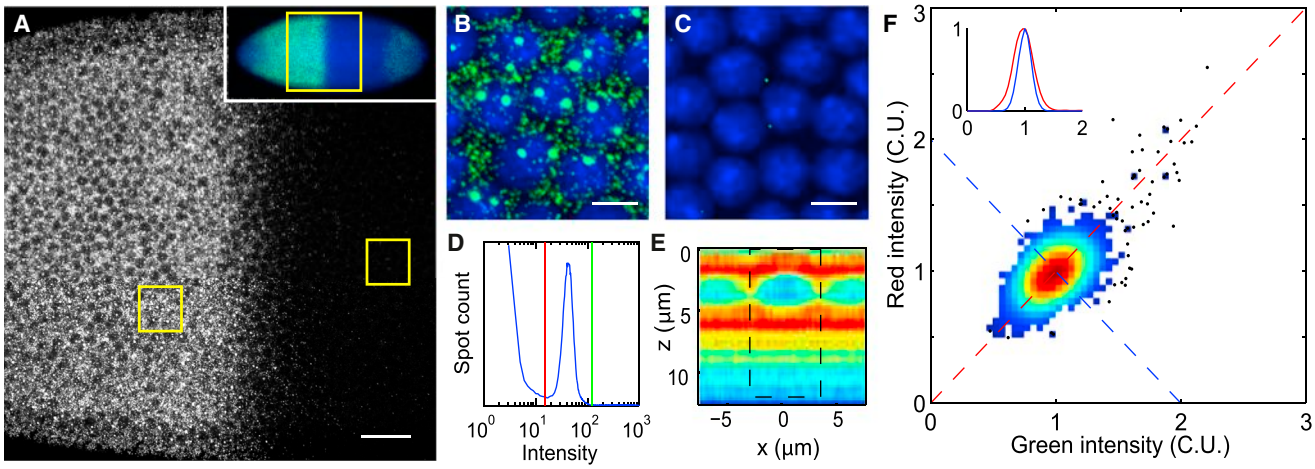

Figure 1. Counting of Absolute Transcript Number in *Drosophila* Embryos

(A) Confocal section through the nuclear layer of a WT embryo during interphase 13 labeled with 114 fluorescent oligonucleotide probes against *hb*, oriented anterior to the left, is shown. Scale bar, 25 μm. Inset is a low-magnification image identifying the region shown in (A).

(B and C) Magnified views of anterior (B) and posterior (C) boxed regions in (A) are presented. hb FISH probes (green) and DAPI staining of DNA (blue). Scale bars, 5 μm.

(D) Particle intensity histogram shows thresholds separating transcripts from noise (red line) and from the long tail of bright transcription sites (green line).

(E) *hb* transcript distribution in axial cross-section through a nucleus centered at x = 0 is shown. z = 0 represents apical surface. Color indicates mean particle density in relative units (red shows high; blue shows low). Dashed box indicates cylindrical summation volume.

(F) Intensity scatterplot in two channels using probes of alternating colors is illustrated. Data point density is given by color; black dots show single point outliers. Inset presents cross-sections of scatterplot in (F) along the correlated (red) and anticorrelated direction (blue) showing Gaussian distributions with σ = 20% (red) and σ = 12% (blue) after normalization to mean cytoplasmic particle intensity (1 "cyto unit" [C.U.]).

See also Figures S1 and S2.

Here, we address these questions with an enhanced method of fluorescence in situ hybridization (FISH) and accompanying image analysis (Little et al., 2011) to label and detect individual zygotically expressed mRNA molecules. We measure in absolute molecular counts the magnitude and fluctuations in the earliest gene expression events of the *Drosophila* embryo. To separate input fluctuations from variability intrinsic to transcription, we focus on those spatial domains in which gene expression is maximally unconstrained. Here, patterning inputs do not determine expression output levels, and thus, input fluctuations cannot impact output variability. These regions thereby reveal the greatest degree of precision achievable by the system. We show that in these regions, the earliest expressed genes share common expression characteristics: despite their expression in spatially distinct territories, their rates of production are identical, and all display intrinsically stochastic transcriptional activity. These similarities suggest that expression rate and variability result from fundamental, global features of transcriptional regulation that limit the attainable degree of precision. Nevertheless, the stochastic expression results in precise and nearly uniform transcript accumulation, achieved by straightforward spatiotemporal averaging.

RESULTS

Measuring Absolute Numbers of mRNA Transcripts in Early *Drosophila* Embryos

Previous work in *Drosophila* embryos has documented that nuclei at similar AP coordinates express nearly equivalent protein amounts of the gap gene Hunchback (Hb) with fluctuations of <10% (Gregor et al., 2007). The transcriptional activator of Hb, Bcd, displays variability on the same order as Hb (Gregor et al., 2007). A precise transcriptional response of the *hb* locus presents the most straightforward though as yet untested explanation of minimal Hb variation. To quantitatively evaluate transcription of *hb*, we adapted a FISH method developed previously (Little et al., 2011) to label *hb* mRNAs using multiple fluorescently labeled antisense DNA oligonucleotides (Figure 1A). By scanning confocal microscopy, we detect two broad classes of objects: sparse, bright spots representing sites of nascent transcription (e.g., Wilkie et al., 1999); and numerous diffraction limited spots, ~90% of which are located in the internuclear space that we refer to as cytoplasmic particles (Figures 1A–1C). These particles exhibit sufficiently high contrast to be readily distinguished from background imaging noise using automated image processing (Figure 1D). Each particle is found on at least three adjacent 250 nm confocal imaging sections with three-dimensional structure identical to the measured point spread function (PSF; Figures S1A–S1D available online). To test detection efficiency, we applied probes with alternating fluorophore colors. A minimum of 85% of cytoplasmic particles detected in one channel are found in the other, indicating that >94% of mRNAs are detected in at least one channel (Figures S1E–S1G).

Tight unimodal clustering around mean intensity suggests that the cytoplasmic particles are similar in mRNA content (Figure 1D). Deviation from mean intensity results from at least two phenomena: particles can be bound by different probe numbers, and multiple particles can overlap and be detected as single

spots. To determine the relative contributions of each, we examined correlation of intensities in two-color detection. Correlation is weak (Figure 1F), implying that the fractional SD of mRNA content in detected particles is at most 16% (see Experimental Procedures). To determine the number of mRNAs per particle, we compared counts of maternally deposited *hb* mRNA particles in entire imaged embryos to those from quantitative RT-PCR (Figure S1H). We found an average of 1.2 ± 0.5 mRNAs per imaged particle. The low mean indicates that the probability of detecting more than two mRNAs per particle is essentially zero. This observation, coupled with the SD in mRNA content from imaging, determines a probability of 97% of finding one mRNA per particle (see Experimental Procedures). Moreover, comparing counts of wild-type (WT) and *hb* hemizygous embryos yields a 2-fold concentration difference (Figure S1I), lending further support to the validity of our approach.

Because the density of zygotically produced *hb* mRNA increases above about one molecule per μm^3, PSFs of individual molecules begin to overlap. We extend particle counting to arbitrarily high density using the naturally large dynamic expression range. We determine counts in dense regions by measuring total fluorescence collected from all mRNAs per volume and calibrating to low-expressing regions where individual mRNAs are counted directly (Figure S2A). We thereby measure absolute concentration and local fluctuation with accuracies of 12% and 5%, respectively (Figures S2B and S2C). The two methods have overlapping domains of applicability: direct counts are accurate for transcript concentrations $\leq$0.5 molecules/μm^3, and total fluorescence for concentrations $\geq$0.35 molecules/μm^3 (Figure S2C). Thus, our FISH method is suitable for high-precision measurements of absolute mRNA counts at any density.

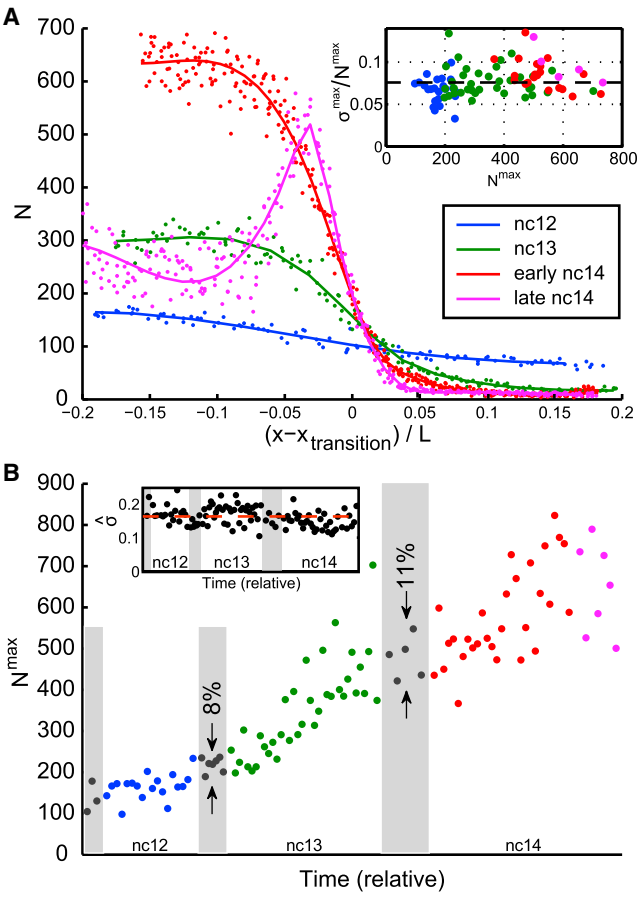

Figure 2. Precision and Reproducibility of Cytoplasmic *hb* Profiles

(A) Absolute cytoplasmic *hb* mRNA counts per standardized volume as a function of AP position are presented. Data for four embryos at nc12 (blue), 13 (green), early 14 (red), and late 14 (magenta) are illustrated. Position is shown as distance from inflection point $x_{transition}$ (see also Figure S3C). Inset presents fractional SD σ^{max}/N^{max} in the spatial domain of highest mRNA accumulation as a function of the mean count (N^{max}) for 101 embryos. Dashed line is at 8%.

(B) Cytoplasmic *hb* mRNA counts (N^{max}) as a function of time is shown. Ages estimated by visual inspection of DAPI staining are illustrated; relative width of mitoses (gray shading) and interphases according to Foe and Alberts (1983) is presented. Reproducibility of counts in 12th and 13th mitoses is 8% and 11%, respectively. Inset shows the estimated reproducibility $\hat{\sigma}$ as a function of time. Data points indicate running averages of root-mean-square displacement from smoothed timeline over 15 consecutive data points normalized to mean. Dashed line represents average $\hat{\sigma}$ (17%).

See also Figure S3.

Cytoplasmic *hb* mRNA and Protein Distributions Display Similar Levels of Precision

To assess fluctuations in transcript number between nuclei, we measure mRNA concentration in cylinders separated by one internuclear distance to a depth of 12 μm beneath the plasma membrane, encompassing the majority of zygotically expressed transcripts (Figures 1E and S3A). As expected from prior observations (e.g., Tautz et al., 1987), *hb* transcripts accumulate dramatically in the embryo anterior during early blastoderm (Figure 2A). Transcription is terminated early in the interphase of nuclear cycle 14 (nc14) except near the embryo midpoint, and maternally supplied transcripts are continuously lost from the posterior (Figures 2A, S3B, and S3C). *hb* mRNA expression profiles correlate well with observed protein levels (Figure S3D).

As an initial quantification of precision, we ascertain the degree of variability independent of putative regulatory inputs by examining the spatial domain of maximal transcript accumulation, i.e., nuclei found in regions of highest-observed gene product levels. Here, expression noise (the fractional SD of *hb* concentration) is 8% ± 2% as early as nc12; thus, *hb* mRNA levels exhibit equal or better precision than Hb protein (Gregor et al., 2007). Age-ordered embryos show a monotonically increasing count through mid-nc14 (Figure 2B), with an approximately constant fractional SD across embryos (17% ± 3%, Figure 2B inset). Ambiguous age determination in fixed samples results in large fluctuations across embryos of approximately the same age. This effect is minimized in embryos undergoing mitosis, during which transcription ceases (Shermoen and O'Farrell, 1991), allowing unambiguously temporal ordering. Counts differed by less than 11% in mitotic embryos, similar to the degree of reproducibility in Hb protein profiles (Gregor et al., 2007). The actual precision and reproducibility are likely to be higher because our measurements contain systematic errors arising from the FISH procedure such as physical distortion (5% measurement error) and error in counts (2%–3% measurement error; see Experimental Procedures and Figure S2C).

Importantly, variation of cytoplasmic profiles is nearly at the level of Poisson counting noise, i.e., at the lowest bound that can be attained by a stochastic process. For 500 molecules per volume, as observed in late nc13 or early nc14, counting noise amounts to 5%, matching the lower bound of our measurements (Figure 2A, inset). Large mRNA counts provide a natural buffer against potential fluctuations in translation that have been observed in other systems (Bar-Even et al., 2006; Newman et al., 2006; Taniguchi et al., 2010), yielding precise Hb expression. By comparison, in genome-wide studies, the most highly (and therefore most precisely) expressed genes in yeast and *E. coli* exhibit cell-to-cell fluctuations exceeding 50% in mRNA count (Gandhi et al., 2011; Taniguchi et al., 2010). Thus, early embryos exhibit an extraordinary degree of precision, rarely observed in other contexts.

Our timeline suggests that *hb* transcript lifetime is large because we see no decrease in counts during the 12th and 13th mitoses (Figure 2B). We verified this by measuring *hb* mRNA lifetime directly, disrupting transcription with α-amanitin injection and subsequently monitoring loss of zygotic *hb* (Figures S3E and S3F). We find a lifetime of $\sim$60 min, consistent with an estimate from imaging: transcript loss of <11% (Figure 2B) in 5 min of mitosis (Foe and Alberts, 1983) corresponds to a lifetime of >45 min. These results show that the accumulation of transcripts is only mildly impacted by degradation.

Determining Instantaneous Transcriptional Activity by Measuring Total Nuclear Nascent mRNA Content

The low noise of *hb* cytoplasmic mRNA counts suggests that nuclei in the fully active region produce transcripts at nearly equivalent rates. However, all systems studied to date, including *E. coli*, yeast, cultured cells, and late *Drosophila* embryos (Golding et al., 2005; Larson et al., 2011; Paré et al., 2009; Raj et al., 2006; Zenklusen et al., 2008), produce transcripts through brief intervals of dense output interspersed with long quiescent periods of stochastic duration (Li and Xie, 2011). This seems incompatible with near uniformity of cytoplasmic mRNA content. To determine the extent of variability in transcriptional activity, we developed a measure of transcription using the fluorescence intensities of nascent transcription sites.

Consistent with previous results from Wilkie et al. (1999), we observe that the maximum number of detectable nascent sites per nucleus increases from DNA replication during interphase from two sites early to four at mid-to-late interphase (Figure S4A). Because sister chromatid loci remain in close physical proximity until mitosis, and because transcription sites occasionally occupy overlapping focal volumes, the number of active loci is challenging to discern. Instead, we used the total fluorescence of all transcription sites in a nucleus as a measure of instantaneous transcriptional activity. Assuming that nascent and mature mRNAs are equally accessible to probes, nascent site intensities can be represented as an equivalent number of mature cytoplasmic mRNAs by normalizing to the mean or "unit" intensity of completed transcripts, yielding transcriptional activity in absolute units of total mRNA content. To determine the extent of measurement error arising from differences in probe binding affinity and/or the subsequent normalization procedure, we used probes of alternating fluorophore colors. Ideally, for a given nascent site, the number of cytoplasmic units (C.U.) will be identical in both colors. Plotting nascent mRNA content of one color as a function of the other yields points on a line with a slope close to unity (among five embryos, the mean slope [±SD] is 0.90 ± 0.09), with a scatter of 5% (Figure 3A). We thus measure transcriptional activity with an error of 5% and relate it to absolute mRNA content with an uncertainty under 20% (the largest deviation of 0.90 ± 0.09 from 1).

Three lines of evidence support the idea that nascent mRNA content reflects instantaneous transcriptional activity. First, the appearance of loci is coupled to the nuclear mitotic cycle: they are observed during interphase and absent during mitosis. Second, transcription in anterior nuclei initiates slightly earlier than in those closer to the center of the embryo, both because anterior nuclei inhabit a region of higher concentration of Bcd and because of metasynchronous nuclear divisions propagating as a wave toward the embryo center (Foe and Alberts, 1983). Consistent with expectation, during the first minute of the 13th interphase, we observe a gradient of nascent mRNA content along the AP axis (Figure S4B). Third, we designed probe sets to label the 5′ and 3′ portions of the completed transcript with fluorophores of green and red colors, respectively. If nascent sites are composed of incomplete transcripts, then 5′ sequences must be more numerous than 3′ sequences (Figure S4C), resulting in an increase of green signal at the expense of red. In agreement, our measurements reveal the enrichment of green signal after normalization (Figure 3B). Importantly, greater 5′ enrichment is observed as the fraction of transcript labeled with green fluorophore increases (increasing slopes of fit lines in Figure 3B). Thus, nascent *hb* loci are largely composed of unfinished transcripts and serve as a measure of transcriptional activity.

Variation in Nascent Transcription Site Activity Is 6-Fold Higher than Variation in Cytoplasmic Output

Given the low noise in cytoplasmic counts, we expected that the nascent mRNA content at all genomic loci would rise simultaneously until saturated with RNA polymerase II (RNAP), in principle reaching and sustaining some maximum nascent mRNA content. However, our measurements of nascent mRNA content show otherwise (Figures 3C–3E). The nuclear nascent mRNA content varies by 22% ± 3%, 3-fold higher than that observed in cytoplasmic counts. To be certain that this variability does not result from the delay in attaining steady-state maximum activity after mitosis (Figure S4D), we confined our analysis to mid and late interphase 13 embryos. We observe this degree of variation even when loci are allowed the full temporal extent of interphase 13 to reach a putative maximum (Figure 3E). These results indicate that *hb* loci fail to sustain any amount of uniform maximum content.

The 22% variation we observe reflects fluctuations across a maximum of four active genomic loci in each nucleus of WT embryos. If transcription from each locus acts independently, then the variability between nuclei must decrease in proportion to the root of the number of loci; thus, the expected variability between individual loci is $22\% \times \sqrt{4} = 44\%$. To test whether loci are in fact independent, we examined embryos heterozygous for a *hb* deficiency in which each nucleus possesses a maximum of only two loci. We observed that total nascent mRNA content

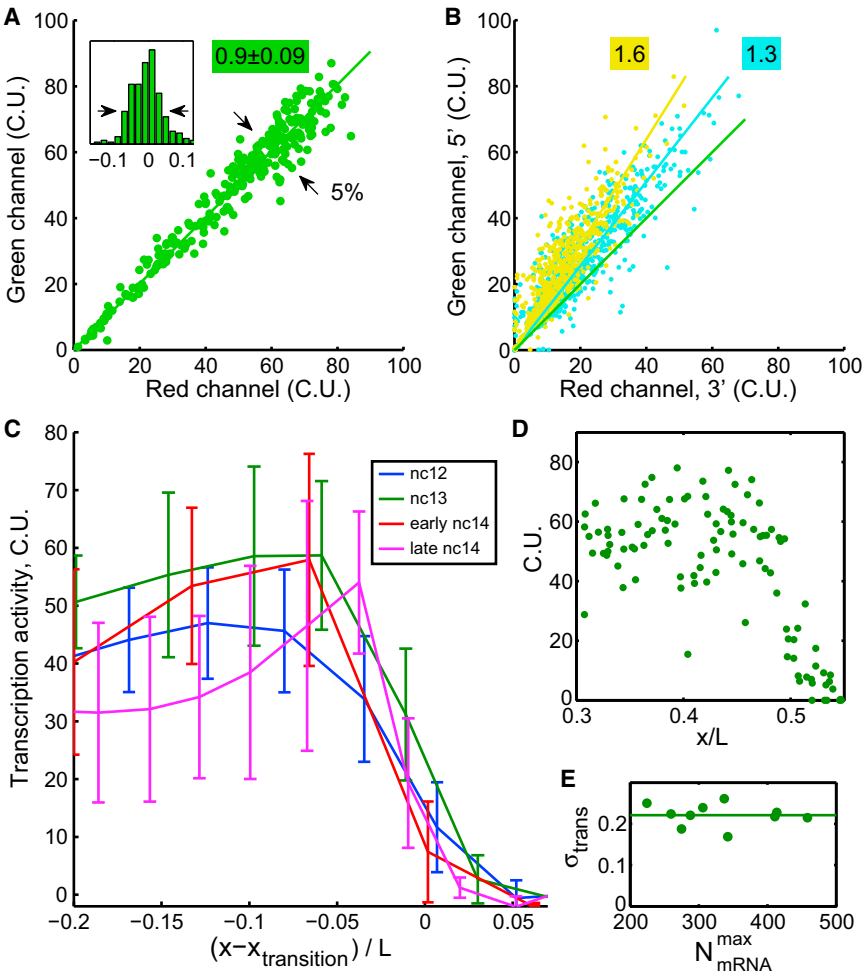

Figure 3. Variability of Transcriptional Activity at Nascent Transcription Sites

(A) Scatterplot of total nascent *hb* mRNA per nucleus using probes of alternating colors for an embryo in nc13 after normalization to the mean cytoplasmic particle intensity (C.U.) is illustrated. Intensities follow a direct proportionality relation with slope 0.90 ± 0.09 (n = 5 embryos). Inset shows root-mean-square normalized deviation from linear fit; scatter = 5% (arrows).

(B) Two-color scatterplot of nascent mRNA content in which probes bearing the same fluorophore are clustered on the 5′ (green channel) and 3′ (red channel) portions of the transcript is shown. Cyan indicates measurements using 57 green and 57 red-labeled probes; observed slope is 1.3. Yellow represents results with 78 green and 36 red-labeled probes; observed slope is 1.6. Green line in (A) is plotted for comparison.

(C) Transcriptional activity per nucleus as a function of position along the AP axis for four embryos in nc12 (blue), 13 (green), 14 early (red), and 14 late (magenta) in binned averages of 10, 20, 40, and 40 nuclei, respectively, is shown. Error bars, SDs within bins. Position is shown as distance from inflection point $x_{transition}$.

(D) Transcriptional activity per nucleus as a function of absolute AP position for the embryo in interphase 13 in (C) is presented.

(E) Transcription noise for ten embryos in nc13 is plotted as fractional SD across nuclei versus cytoplasmic *hb* counts within the spatial domain of highest accumulation. Transcription activity noise remains constant throughout interphase at 22% ± 3%.

See also Figure S4.

per nucleus varies by 33% ± 6%, which corresponds to a transcriptional activity of $33\% \times \sqrt{2} = 47\%$ in individual loci. This number is nearly identical to WT and, hence, consistent with independence. The variability between individual loci of ~45% represents a 6-fold increase over fluctuations in cytoplasmic counts. Analyzing closely apposed alleles on sister chromatids with sufficient separation to reliably gauge intensities reveals no correlation in their activities (Figure 4A), indicating independent activity even for recently duplicated loci. If the observed fluctuations result from variability in any input factor controlling *hb* expression (i.e., "extrinsic" noise), then the variation in total nuclear activity would show no dependence on the number of loci in the nucleus. However, because the noise scales with the number of loci (Figure 4B), the fluctuations we observe in the maximally expressed domain are intrinsic to the process(es) of transcription and not determined by variability in the controlling inputs.

Transcriptional activity will necessarily exhibit some degree of noise arising from stochastic single-molecule events, but the fluctuations we observe exceed the Poisson expectation considerably. From our observations, we can estimate the number of RNAPs engaged in transcription per nucleus and thereby determine the expected degree of fluctuations; we find the predicted noise magnitude of at most 11% (see Experimental Procedures). The observed fluctuations of 22% ± 3% are at least 2-fold greater than this prediction, ruling out a model in which transcriptional fluctuations in the region of maximum expression are determined by a single rate-limiting step of RNAP loading (Figure S4C).

From these observations, we conclude that first, even in the domain of maximal expression, *hb* is not saturated with the maximum possible density of RNAP, and second, despite the near uniformity of cytoplasmic transcript concentration, instantaneous activity of individual *hb* loci is intrinsically stochastic. The estimated variation in transcriptional activity at an individual locus is very similar to the minimum value of ~50% observed for differences in mRNA numbers for the most highly expressed genes in yeast and *E. coli* (Gandhi et al., 2011; Taniguchi et al., 2010). In all contexts, variation between cells is significantly higher than that predicted for a process with a single rate-limiting step (Chubb et al., 2006; Golding et al., 2005; Le et al., 2005; Raj et al., 2006). These similarities across such diverse contexts suggest that the observed fluctuations are globally inherent features of the activity of otherwise "fully activated" genes. In the context of a rapidly developing embryo, the highest-attainable

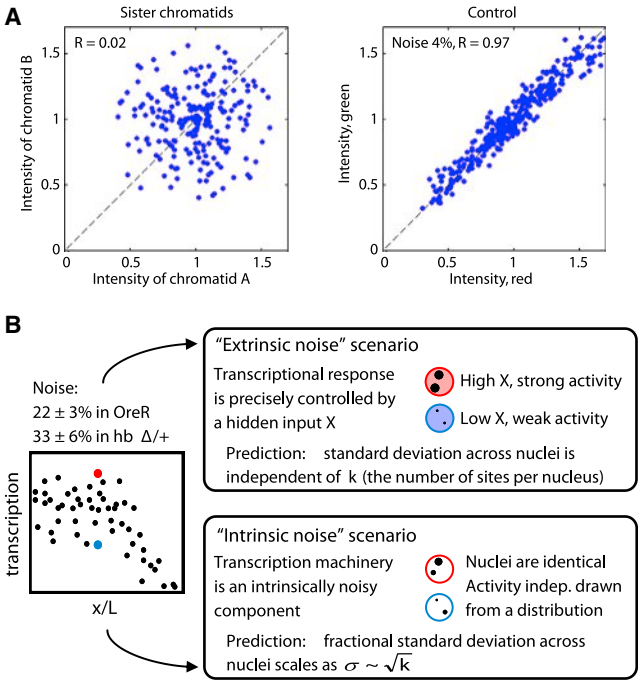

Figure 4. Fluctuations in *hb* Transcription Are Dominated by Intrinsic Noise

(A) Transcriptional activity of loci on optically resolved sister chromatids is uncorrelated (Pearson correlation coefficient R = 0.02), compared to the tight correlation (R = 0.97) in a control experiment using probes of alternating colors (with 4% imaging noise).

(B) Transcriptional variability arises from fluctuations in inputs (extrinsic noise) and from the process of transcription itself (intrinsic noise). Two extreme scenarios are presented in cartoon form. Upper: a fluctuating extrinsic input leads to correlated activities of transcription sites within a given nucleus; its contribution to the fractional SD is independent of the number of transcribing loci k. Lower: intrinsic mechanistic noise affects all transcription sites independently; the fractional SD scales as the inverse square root of available transcription sites. Left view shows the measured transcription noise in WT and *hb*Δ/+ embryos (22% ± 3% and 33% ± 6%, respectively) showing scaling behavior characteristic of intrinsic noise with magnitude ~45% ($\sqrt{4} * 22\% = 44\%$; $\sqrt{2} * 33\% = 47\%$).

expression rate would serve to minimize cell-to-cell fluctuations to the fullest possible extent and thereby promote precision. The observed tolerance of fluctuations, linked with the apparent inability to sustain saturating RNAP density, suggests that this degree of imprecision cannot be circumvented even in this highly precise developmental context.

The Magnitude of Expression Noise Is Independent of Autoregulation and Transcriptional Modulation

Our results suggest that in addition to fluctuations from controlling inputs, *hb* activity possesses a large inherently stochastic component. We examined whether the inherent noise could be attributed to features of *hb* regulation. First, the *hb* locus contains several binding elements for Hb protein itself, and genetic evidence indicates that Hb is required for its own expression (Holloway et al., 2011; Margolis et al., 1995; Treisman and Desplan, 1989). Positive feedback will amplify fluctuations if locally produced mRNA and protein dominate autoregulation (i.e., if diffusion is limited). Second, noise necessarily decreases as RNAPs approach their maximum loading density along the gene, but transcriptional repressors might disallow high densities, resulting in greater variability.

To determine the effect of positive feedback, we examined mRNA production in embryos homozygous for an early *hb* stop codon. Mutants and WT siblings display similar expression patterns until mid-nc14 when WT embryos show reduced anterior expression and the loss of accumulated transcripts (Figures 5A and 5B). In mutants, *hb* is maintained, resulting in continued high transcript density at late times (Figure 5A; Margolis et al., 1995). However, the absence of autoinhibition did not alter the magnitude of variation in transcriptional activity compared to WT siblings, supporting the idea of intrinsic fluctuations and suggesting that zygotic Hb inhibits its own expression (Li et al., 2008; Perry et al., 2012; Treisman and Desplan, 1989).

We also examined whether the removal of transcriptional inhibitors would allow the accumulation of larger numbers of RNAP. First, we examined *hb* expression in *runt* homozygous mutants because Runt is implicated in gap gene regulation (Chen et al., 2012; Li et al., 2008;Tsai and Gergen, 1994). *hb* expression differs from WT starting at mid-nc14 when *runt* embryos maintain high levels of *hb* transcript in the anterior 20%–40% (Figure 5C). *hb* profiles in *runt* mutants tend to resemble younger WT siblings, reaching WT levels near the end of nc14 (Tsai and Gergen, 1994), suggesting a delay in the reduction of anterior expression. In support, we find that *runt* mutants express slightly greater transcriptional activity than WT embryos with similar expression profiles (Figure 5D). However, at no time does expression noise differ noticeably from WT. Therefore, *runt* activity is required for the correct timing of *hb* downregulation but plays no discernable role in determining fluctuations in transcriptional activity.

Finally, we tested the effect of manipulating the activity of maternally provided transcriptional modulators. We impaired the activity of the repressors Capicua and the corepressor Groucho by mutation and observed that although *hb* expression boundaries were altered consistent with previous observations (e.g., Margolis et al., 1995), *hb* expression noise in the anterior was not affected. We also altered the genetic dosage of *bcd* to provide between 50% and 280% of WT activity, which shifted *hb* expression along the AP axis as expected (Liu et al., 2013) but had no effect on expression variability (Figures S5A and S5B). Thus, our data are consistent with the view that the fluctuations in *hb* transcriptional activity arise from intrinsically stochastic processes, independent of variability in transcriptional modulators.

Gap Genes Share Expression Characteristics and Are Produced at Equal Rates

hb transcription fluctuates around a mean polymerase density that is about half the level that is physically obtainable. What sets the magnitude of the mean activity? Specific features of the *hb* promoter may limit activity. Alternatively, the maximum rate may not be specific to *hb* but shared among early expressed genes. If so, this would suggest that the maximum obtainable output, and its related noise level, is not set by any specific

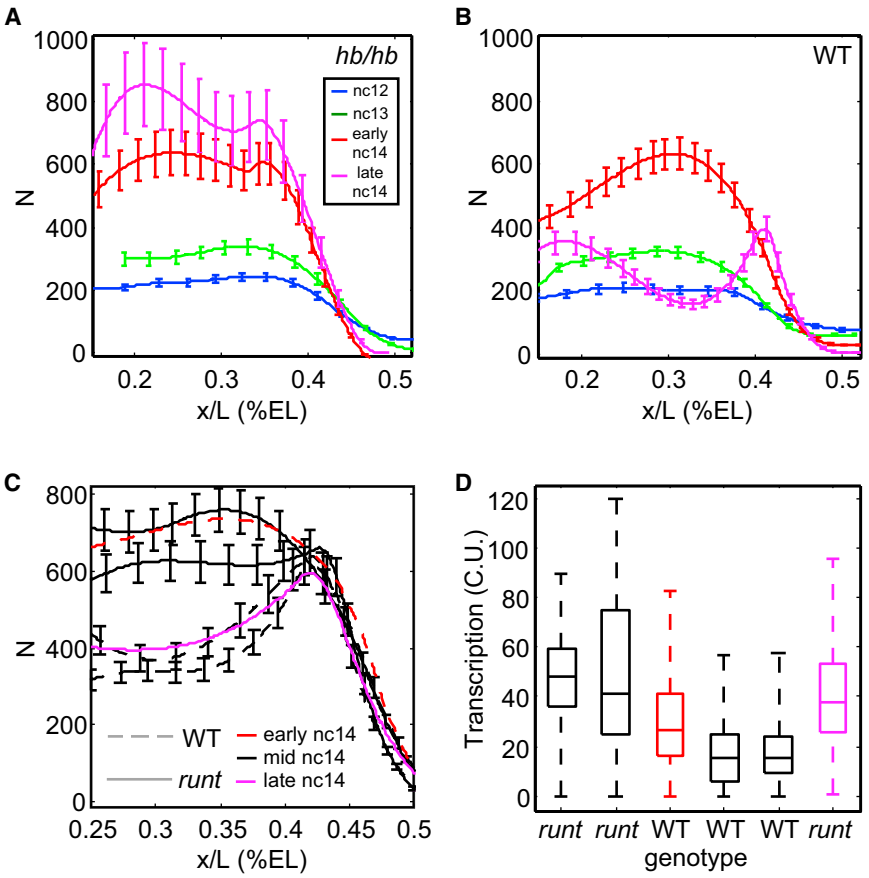

Figure 5. Mutations in *hb* and *runt* Impair Timely Repression of *hb* Expression

(A and B) Cytoplasmic *hb* mRNA counts per standardized volume as a function of AP position of similarly staged zygotic *hb* mutants (A) and WT siblings (B) are presented. Smooth profiles are best spline fits. Error bars are root-mean-square deviations from smoothened profiles, calculated in windows of ten nuclei.

(C and D) *runt* mutants show delayed repression of *hb* transcription in nc14.

(C) Solid lines indicate *runt* mutants; dashed lines show WT siblings. Black represents embryos of similar age (mid nc14) as judged by DAPI. Profile of an early nc14 WT embryo (red line) resembles midstage *runt* mutants, whereas a very late *runt* mutant (magenta line) is similar to earlier WT siblings.

(D) Transcriptional activity in anterior nuclei of the embryos shown in (C) is presented. Box plot depicts median, quartiles, and range of nascent transcription site activity for each embryo. *runt* mutants display consistently higher *hb* activity compared to WT siblings, leading to the inappropriately high *hb* transcript counts at late times as shown in (C).

See also Figure S5.

promoter-enhancer arrangement or any patterning cue and, instead, is determined by general physical considerations.

To discern between these possibilities, we measured the accumulation of transcripts of four gap genes primarily responsible for trunk patterning: *hb*, *Krüppel* (*Kr*), *knirps* (*kni*), and *giant* (*gt*) (Figure 6A). We found that all four genes display nearly uniform accumulation of cytoplasmic mRNAs accompanied by over 3-fold higher fluctuations in instantaneous transcriptional activity, essentially identical to the characteristics of *hb* (Figures 6B and 6C). These results strongly suggest that all early transcriptional events are subject to common constraints.

To closely compare transcript accumulation between genes, we took advantage of the observation that for *Kr* and *kni*, cytoplasmic mRNA density increases monotonically between early nc12 and well into interphase 14 (Figures S5C and S5D), in contrast to *hb*, which ceases accumulating broadly in early nc14 (Figure 2A). We used counts of *Kr* or *kni* as a proxy for time, reducing staging uncertainty when comparing different genes. We performed dual-color labeling with probes against pairs of gap genes and report cytoplasmic counts of *hb*, *gt*, and *kni* mRNA as a function of *Kr* (Figure 6).

Figure 6C displays the expression of *hb* and *Kr* in WT (blue), *hb* hemizygous (green), and Kr^1 heterozygous (red) embryos during nc12 and nc13. Counts in deficiency or mutant heterozygous embryos deviate considerably from WT (Figure 6C, inset), but after multiplying the counts of the deficient gene by 2, all points collapse onto the same line (Figure 6C), showing the absence of compensatory mechanisms. We observed the same behavior for *gt-Kr* and *kni-Kr* expression pairs. Unexpectedly, for the three sets of gene pairs, linear fitting yields lines with slopes between 0.9 and 1.15 (Figure 6E); that is, in their regions of maximal expression, the four genes are produced at nearly identical rates. The differences between absolute levels within these regions (Figure 6E) reflect differences in the timing of when *kni*, *Kr*, and *gt* transcripts begin to accumulate, and for *hb* the perdurance of maternal mRNA. These maximal production rates are independent of Bcd activator concentration: although genetically altering the dosage of *bcd* between 50% and 280% of WT shifts the expression domains along the AP axis (Liu et al., 2013), this manipulation does not alter either accumulation rate or precision (Figures S5A and S5B).

These results are consistent with the idea that these transcripts are produced at the same rate. This strong similarity occurs despite the fact that these genes are expressed maximally in nonoverlapping spatial domains. The transcriptional activity in the maximally expressed domain and the magnitude of transcriptional noise are therefore set independently of the inputs that determine spatially patterned expression, which are specific to each gene. By focusing on the regions of maximal expression, we could isolate the features of transcription that appear to be universal across gap genes and, furthermore, match the noise characteristics previously observed in bacteria and cell cultures. This suggests that the failure to sustain a maximal loading of RNAPs on

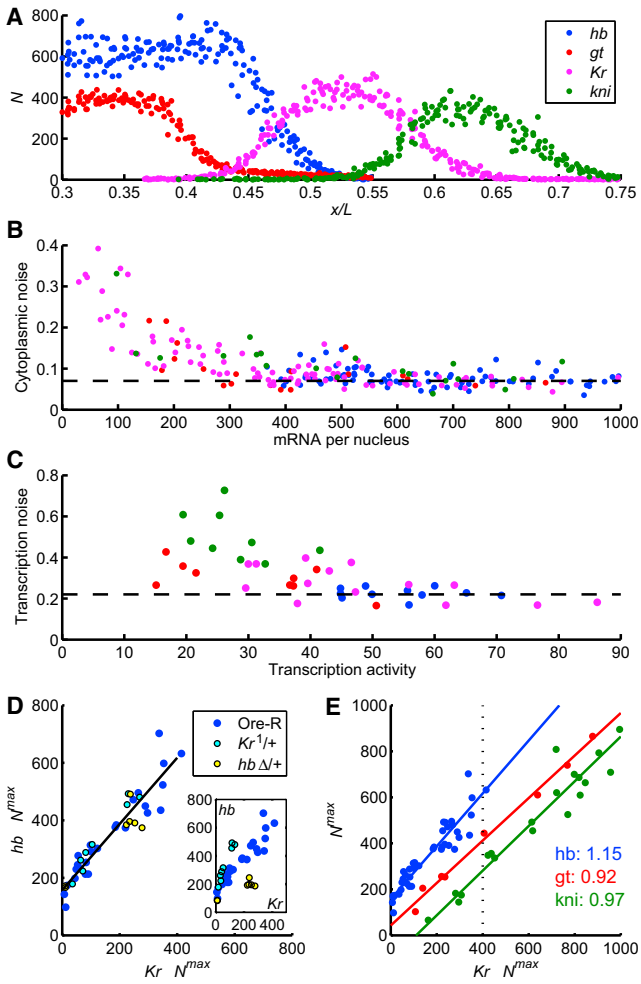

Figure 6. Universal Properties of Gap Gene Transcription

(A) Cytoplasmic profiles are shown for four gap genes (mRNA concentration per standard volume as a function of AP position) measured in two embryos of the same age (second half of nc13; indicated by dotted line in E) processed with *hb* (blue) and *gt* (red) and with *Kr* (magenta) and *kni* (green) probes.

(B–E) Gap gene expression characteristics within each gene's region of maximum expression are presented.

(B) Noise in cytoplasmic counts as a function of counts per nucleus (dashed line indicates 8%) is illustrated.

(C) Noise in transcriptional activity as a function of activity level (dashed line indicates 23%) is shown.

(D) mRNA expression (mean mRNA count per standard volume) in embryos from cycle 12 to early 14 costained with FISH probes against *hb* and *Kr* mRNA is illustrated. Data from WT embryos (blue) coincides with those from embryos deficient for one copy of *hb* (*hb*Δ/+; yellow) or *Kr* (Kr^1/+; cyan) when the concentration of the respective mRNA is rescaled by a factor of 2. Inset shows raw data (not rescaled).

(E) Levels of *hb* (blue), *kni* (green), and *gt* (red) versus *Kr* are shown. Data from WT, *hb*Δ/+, and Kr^1/+ embryos are combined by rescaling as in (D) (also see Figures S5C and S5D). *hb* data as in (A) are presented; *kni* and *gt* were assessed in cycles 13 and 14. Slopes of fit lines indicate ratio of absolute production rates; all are within 15% of unity.

the gene and the intrinsic noise of 45% are a common feature of transcriptional activation across diverse biological contexts.

DISCUSSION

The fundamental question of how embryos achieve precise control over the earliest transcriptional events is largely unanswered. General models of embryogenesis posit that early developmental events are dominated by molecular noise and imprecision in the control of gene expression (Arias and Hayward, 2006; Manu et al., 2009; Rao et al., 2002), a view consistent with observations of wide fluctuations in transcriptional activity in the majority of systems assayed quantitatively (Li and Xie, 2011). Indeed, the finding in fly embryos that instantaneous transcriptional activity varies between loci by nearly 50% suggests that early transcription in fly embryos obeys rules of stochastic activity observed in other systems where output can vary by a similar degree and is often much higher (Munsky et al., 2012). Stochastic variation appears to be a universal feature of transcription from single-cell organisms grown in culture (Raj et al., 2006; So et al., 2011; Stewart-Ornstein et al., 2012) and for cells in certain developmental settings (Paré et al., 2009; Raj et al., 2010; Saffer et al., 2011). *Drosophila* embryos display an extraordinary degree of precision in the rapid establishment of distinct gene expression programs; nevertheless, even this system cannot circumvent stochastic transcriptional activity. This finding supports the idea that control systems that might overcome stochastic molecular activity are difficult to design, costly to implement, and rarely if ever found (Lestas et al., 2010).

It is possible that cultured yeast and bacteria exist at sufficiently high densities such that precision is not required to ensure survival of a large fraction of the population; indeed, in several cases, stochastic expression serves to maximize survival options (Balaban et al., 2004; Maamar et al., 2007; Mirouze et al., 2011; Nachman et al., 2007). In addition, for prokaryotes and haploid yeast and unlike early embryos, the presence of a single genomic locus precludes the possibility of noise filtering by averaging over independent loci. Alternatively, precision might be required to ensure the survival of single-cell organisms when grown in their endogenous conditions, which may be difficult to study in a laboratory setting. However, in stark contrast to single-cell organisms, many developing embryos possess large fields of cells that must coordinately undertake rapidly determined fate decisions, thus mandating high precision and low expression noise such that the appropriate gene expression programs are induced at the correct time and place. If in *Drosophila* patterning mRNAs accumulate in a precise manner minimizing expression noise, as we have shown here, how then can the embryo achieve this near uniformity?

Spatiotemporal Averaging Reconciles Highly Variant Transcription with Precise Accumulation and Recovers the Input-Output Relationship

Large differences in nascent transcript content sustained over sufficiently long periods would inevitably result in unequal transcript production, inconsistent with nearly homogeneous cytoplasmic transcript concentration. As noted above, the long lifetime of *hb* transcripts allows substantial accumulation during the course of the syncytial blastoderm stage. If instantaneous nascent mRNA content is not maintained continuously during

interphase but instead fluctuates about the mean as a result of varying RNAP number, then cytoplasmic accumulation serves as a natural time-averaging filter. The impact of time averaging can be estimated in two independent ways. First, transcript accumulation reflects temporal integration of a signal fluctuating with a characteristic time t_0, the time it takes a polymerase to traverse the 3.2 kbp of the hb gene. RNAP processivity is estimated at 1.1–1.4 kbp/min (Irvine et al., 1991; O'Brien and Lis, 1993; Shermoen and O'Farrell, 1991; Thummel et al., 1990), providing a rough estimate consistent with the observed noise filtering (see Extended Experimental Procedures). Alternatively, a more careful estimate (Figure S6B) yields a theoretical bound on the maximum efficiency of temporal averaging based on directly measured quantities, most crucially, the absolute number of engaged polymerases per nucleus. In the case of *Kr* mRNA profile, by the time the mean expression level reaches 800 molecules per nucleus, pure temporal averaging can at most reduce the expression noise to 8%. For these late embryos, however, our measurements show a consistently lower noise level of 6% ± 2%, suggesting an additional noise-filtering mechanism.

Additional filtering can be readily provided by a small degree of spatial averaging by the exchange of mRNA between neighboring cytoplasmic volumes before the partitioning of the syncytial blastoderm. mRNA possesses some mobility: both *hb* and *Kr* transcript numbers increase at >10 μm from their sites of production in nuclei (Figures S3A and S6A). We note that cylindrical summation volumes with a diameter of one internuclear distance contact each other, so that the mRNA traveling distance required to observe spatial averaging is very small. A straightforward estimate (see Extended Experimental Procedures) shows that attributing the excess noise filtering to spatial averaging requires only 4% of produced transcripts to be exchanged between neighboring volumes. Thus, even a limited degree of spatial averaging is completely sufficient to account for the appearance of low variation in cytoplasmic accumulation from stochastic transcription.

These results have several implications. First, we note that the observed variation in cytoplasmic concentration is likely to contain error introduced by our measurement, and the variation we observe is nearly at the level of counting noise. This might indicate that spatial averaging predominates the filtering of transcription noise; however, the degree to which RNAP numbers fluctuate and, therefore, the extent of purely temporal averaging can only be determined with measurements in living embryos. Second, both spatial and temporal averaging mechanisms effectively relax a requirement for rapid, tightly controlled transcriptional responses to modulating inputs, thereby minimizing the need for additional layers of feedback or other control systems. In turn, the fluctuations of putative inputs must approach the same degree of noise as the intrinsic variability of the transcriptional process itself before any effect on gene expression is realized.

It is well established that the position of the Hb expression boundary depends on Bcd genetic dosage (Driever and Nüsslein-Volhard, 1988) and that the concentration of Hb protein along the AP axis depends upon and is at least as precise as Bcd concentration (Gregor et al., 2007). Superficially, a highly stochastic transcriptional response would appear to render irrelevant any link between Bcd precision and Hb output: the 10% fluctuations observed for Bcd (Gregor et al., 2007) cannot directly impact a transcriptional process whose noise is >40%. However, each nucleus employs averaging mechanisms reducing the effect of intrinsic noise. Because of the central role played by time averaging, the relative importance of various noise sources depends on the timescale of observation. The immediate readout (on a scale of minutes) is dominated by intrinsic transcriptional noise that renders the precision of the input irrelevant. Averaging over active loci, over time, and between neighboring nuclei, the contribution of intrinsic noise becomes comparable with the input (or extrinsic) fluctuations. Thus, on a long timescale, such as 3 hr of development, the precision of patterning decisions becomes limited by the extrinsic variability. A precise response to Bcd will be recovered as long as the mean activity of *hb* transcription is correlated with Bcd concentration, as proposed previously by Erdmann et al. (2009). This reconciles the apparently stochastic behavior of *hb* transcriptional activity with the precisely positioned boundary of expression (Porcher et al., 2010). In this manner, Hb activity and fluctuations in the boundary domain retain the previously observed dependence upon levels of and fluctuations in Bcd concentration.

Limitations to Precise Control of Gene Expression

We have shown that in the context of the gap genes, transcript output in the maximally expressing region does not equate with the actual maximum attainable density of RNAP loading. This maximum is attained by only a small fraction of nuclei at any given moment. Thus, it is currently unclear what determines the mean density of RNAP loading common to these four genes and what prohibits all nuclei from continuously activating the achievable maximum density. It is possible that the output rate is determined by a common, maternally supplied and spatially ubiquitous factor, for example Zelda or BSF (De Renzis et al., 2007; Liang et al., 2008), which calibrates the RNAP density of these four genes to give rise to the observed transcript output rate. Conversely, from the perspective of noise minimization, it would seem advantageous to design these genes' promoter-enhancer architecture such as to obtain the actual maximum possible density because higher output achieves greater noise reduction. However, a biological system likely cannot be readily engineered to produce transcripts at an arbitrarily rapid rate. Hence, it seems likely that mean RNAP loading, and hence transcript output, is strongly influenced by physical considerations, such as transcription factor binding, promoter melting, enhancer looping, and/or chromatin accessibility, that might be difficult to overcome by any simple means. Future work will determine the extent to which the mean polymerase density we observe for these four genes is a shared feature of early expression and the extent to which this rate can be manipulated according to cellular context. Moreover, further studies will be required to determine the timescale of fluctuations of an active locus during interphase, i.e., whether variations arise largely from "bursts" of dense RNAP loading followed by quiescent periods, or conversely, if the variations result from RNAP-loading rates that are maintained continuously during interphase but differ dramatically between loci.

The formation of cellular membranes during the 14th interphase prohibits spatial exchange. It is thus improbable that spatial averaging mechanisms can play a role in ensuring precise responses at this time. Moreover, the transcripts of the pair-rule genes are directed to the apical surface where they accumulate (Davis and Ish-Horowicz, 1991). Differential cellular behavior, presaging the formation of morphological structures, emerges in the latter part of the 14th interphase. Thus, it is likely that shortly after the onset of the 14th interphase, individual cells begin accumulating gene products required for their specific behaviors, thus rendering spatial averaging a hindrance to differentiation. It is therefore likely that temporal averaging and/or other mechanisms such as regulatory feedback ensure the precise distribution of patterning factors at this time. The degree of precision of transcriptional events over the course of the 14th interphase will be the subject of future investigations.

EXPERIMENTAL PROCEDURES

Fly Strains and Embryo Manipulation

Oregon-R (Ore-R) embryos were used as WT. α-Amanitin injection was performed as described by Edgar et al. (1986). RT-qPCR method is described in the Extended Experimental Procedures. Embryos heterozygous for a deficiency spanning *hb* or for the mRNA null Kr^1 mutation were collected from crosses of heterozygous adults (w^{1118}; Df(3R)BSC477/TM6C and Kr^1/SM6) and distinguished from homozygous mutant and homozygous balancer siblings by visual inspection of nascent mRNA sites. Homozygous hb^{12} mutants were obtained from crosses of heterozygous adults carrying a TM3 balancer marked with *hb-lacZ* reporter and identified by the absence of *lacZ* expression. *runt* mutant embryos were collected from crosses of a deficiency-bearing stock (Df(1)BSC645, w^{1118}/Binsinscy) and mutants distinguished by the absence of *runt* expression using FISH probes. gro^{MB36} germline clones were generated using the FLP-FRT recombinase system (Ajuria et al., 2011; Xu and Rubin, 1993). cic^1 homozygous females were crossed to WT males to assay the effect of disabling *capicua* activity.

FISH and Imaging

Embryos were fixed in 5% formaldehyde, 1X PBS for 20 min, and devitellinated as described by Lécuyer et al. (2008). Fixed embryos were rinsed three times in 1X PBS and washed for 10 min in smFISH wash buffer (4X SSC, 35% formamide, 0.1% Tween 20). Hybridization to probes complementary to the reading frame of *hb*, *Kr*, *kni*, or *gt* and conjugated to Atto 565 (Sigma-Aldrich; 72464) or Atto 633 (Sigma-Aldrich; 01464) was performed for 16–24 hr at a concentration of about 1 nM per probe in hybridization buffer (4X SSC, 35% formamide, 10% dextran sulfate, 2 μg/ml BSA [NEB; B9001], 0.1 mg/ml salmon sperm DNA [Invitrogen; 15632-011], and 2 mM ribonucleoside vanadyl complex [NEB; S1402S], 0.1% Tween 20). After two washes of 1 hr in wash buffer, embryos were rinsed twice briefly in 1X PBS, stained with DAPI, and mounted in VECTASHIELD (Vector Laboratories; H-1000). For combined FISH and immunofluorescence, incubation in *hb*-Atto-565 probes was reduced to 2 hr. Hb antibody staining was performed as described by Dubuis et al. (2013) with rat anti-Hb and goat anti-rat Alexa 647. Imaging was performed by laser-scanning confocal microscopy on a Leica SP5 inverted microscope as described (Little et al., 2011) except that we used a 63× HCX PL APO CS 1.4 NA oil immersion objective with pixels of 76 × 76 nm and z spacing of 250 nm. We typically obtained stacks representing 20 μm in total axial thickness starting at the embryo surface. Image analysis was performed as described (Little et al., 2011) with enhancements described in the Extended Experimental Procedures.

SUPPLEMENTAL INFORMATION

Supplemental Information includes Extended Experimental Procedures and six figures and can be found with this article online at http://dx.doi.org/10.1016/j.cell.2013.07.025.

ACKNOWLEDGMENTS

We gratefully acknowledge E. Wieschaus for insightful discussions and continuous support. We thank W. Bialek, S. Blythe, B. Chun, G. Deshpande, S. Di Talia, H. Garcia, S. Kyin, M. Petkova, R. Samanta, T. Schupbach, G. Tkacik, and the Bloomington Drosophila Stock Center. This work was supported by NIH Grants P50 GM071508 and R01 GM097275, and by Searle Scholar Award 10-SSP-274 to T.G.

Received: January 13, 2013
Revised: May 20, 2013
Accepted: July 12, 2013
Published: August 15, 2013

REFERENCES

Ajuria, L., Nieva, C., Winkler, C., Kuo, D., Samper, N., Andreu, M.J., Helman, A., González-Crespo, S., Paroush, Z., Courey, A.J., and Jiménez, G. (2011). Capicua DNA-binding sites are general response elements for RTK signaling in *Drosophila*. Development *138*, 915–924.

Arias, A.M., and Hayward, P. (2006). Filtering transcriptional noise during development: concepts and mechanisms. Nat. Rev. Genet. *7*, 34–44.

Balaban, N.Q., Merrin, J., Chait, R., Kowalik, L., and Leibler, S. (2004). Bacterial persistence as a phenotypic switch. Science *305*, 1622–1625.

Bar-Even, A., Paulsson, J., Maheshri, N., Carmi, M., O'Shea, E., Pilpel, Y., and Barkai, N. (2006). Noise in protein expression scales with natural protein abundance. Nat. Genet. *38*, 636–643.

Chen, H., Xu, Z., Mei, C., Yu, D., and Small, S. (2012). A system of repressor gradients spatially organizes the boundaries of Bicoid-dependent target genes. Cell *149*, 618–629.

Chubb, J.R., Trcek, T., Shenoy, S.M., and Singer, R.H. (2006). Transcriptional pulsing of a developmental gene. Curr. Biol. *16*, 1018–1025.

Cohen, A.A., Kalisky, T., Mayo, A., Geva-Zatorsky, N., Danon, T., Issaeva, I., Kopito, R.B., Perzov, N., Milo, R., Sigal, A., and Alon, U. (2009). Protein dynamics in individual human cells: experiment and theory. PLoS One *4*, e4901.

Davis, I., and Ish-Horowicz, D. (1991). Apical localization of pair-rule transcripts requires 3′ sequences and limits protein diffusion in the *Drosophila* blastoderm embryo. Cell *67*, 927–940.

De Renzis, S., Elemento, O., Tavazoie, S., and Wieschaus, E.F. (2007). Unmasking activation of the zygotic genome using chromosomal deletions in the *Drosophila* embryo. PLoS Biol. *5*, e117.

Driever, W., and Nüsslein-Volhard, C. (1988). The bicoid protein determines position in the *Drosophila* embryo in a concentration-dependent manner. Cell *54*, 95–104.

Dubuis, J.O., Samanta, R., and Gregor, T. (2013). Accurate measurements of dynamics and reproducibility in small genetic networks. Mol. Syst. Biol. *9*, 639.

Edgar, B.A., Weir, M.P., Schubiger, G., and Kornberg, T. (1986). Repression and turnover pattern fushi tarazu RNA in the early *Drosophila* embryo. Cell *47*, 747–754.

Erdmann, T., Howard, M., and ten Wolde, P.R. (2009). Role of spatial averaging in the precision of gene expression patterns. Phys. Rev. Lett. *103*, 258101.

Foe, V.E., and Alberts, B.M. (1983). Studies of nuclear and cytoplasmic behaviour during the five mitotic cycles that precede gastrulation in *Drosophila* embryogenesis. J. Cell Sci. *61*, 31–70.

Gandhi, S.J., Zenklusen, D., Lionnet, T., and Singer, R.H. (2011). Transcription of functionally related constitutive genes is not coordinated. Nat. Struct. Mol. Biol. *18*, 27–34.

Gergen, J.P., Coulter, D., and Wieschaus, E. (1986). Segmental pattern and blastoderm cell identities. In Gametogenesis and the Early Embryo, J.G. Gall, ed. (New York: Liss), pp. 195–220.

Golding, I., Paulsson, J., Zawilski, S.M., and Cox, E.C. (2005). Real-time kinetics of gene activity in individual bacteria. Cell *123*, 1025–1036.

Gregor, T., Tank, D.W., Wieschaus, E.F., and Bialek, W. (2007). Probing the limits to positional information. Cell *130*, 153–164.

Holloway, D.M., Lopes, F.J., da Fontoura Costa, L., Travençolo, B.A., Golyandina, N., Usevich, K., and Spirov, A.V. (2011). Gene expression noise in spatial patterning: hunchback promoter structure affects noise amplitude and distribution in *Drosophila* segmentation. PLoS Comput. Biol. *7*, e1001069.

Irvine, K.D., Helfand, S.L., and Hogness, D.S. (1991). The large upstream control region of the *Drosophila* homeotic gene Ultrabithorax. Development *111*, 407–424.

Kaern, M., Elston, T.C., Blake, W.J., and Collins, J.J. (2005). Stochasticity in gene expression: from theories to phenotypes. Nat. Rev. Genet. *6*, 451–464.

Kornberg, T.B., and Tabata, T. (1993). Segmentation of the *Drosophila* embryo. Curr. Opin. Genet. Dev. *3*, 585–594.

Lagha, M., Bothma, J.P., and Levine, M. (2012). Mechanisms of transcriptional precision in animal development. Trends Genet. *28*, 409–416.

Lander, A.D. (2013). How cells know where they are. Science *339*, 923–927.

Larson, D.R., Zenklusen, D., Wu, B., Chao, J.A., and Singer, R.H. (2011). Real-time observation of transcription initiation and elongation on an endogenous yeast gene. Science *332*, 475–478.

Le, T.T., Harlepp, S., Guet, C.C., Dittmar, K., Emonet, T., Pan, T., and Cluzel, P. (2005). Real-time RNA profiling within a single bacterium. Proc. Natl. Acad. Sci. USA *102*, 9160–9164.

Lécuyer, E., Parthasarathy, N., and Krause, H.M. (2008). Fluorescent in situ hybridization protocols in *Drosophila* embryos and tissues. Methods Mol. Biol. *420*, 289–302.

Lestas, I., Vinnicombe, G., and Paulsson, J. (2010). Fundamental limits on the suppression of molecular fluctuations. Nature *467*, 174–178.

Li, G.W., and Xie, X.S. (2011). Central dogma at the single-molecule level in living cells. Nature *475*, 308–315.

Li, X.Y., MacArthur, S., Bourgon, R., Nix, D., Pollard, D.A., Iyer, V.N., Hechmer, A., Simirenko, L., Stapleton, M., Luengo Hendriks, C.L., et al. (2008). Transcription factors bind thousands of active and inactive regions in the *Drosophila* blastoderm. PLoS Biol. *6*, e27.

Liang, H.L., Nien, C.Y., Liu, H.Y., Metzstein, M.M., Kirov, N., and Rushlow, C. (2008). The zinc-finger protein Zelda is a key activator of the early zygotic genome in *Drosophila*. Nature *456*, 400–403.

Little, S.C., and Wieschaus, E.F. (2011). Shifting patterns: merging molecules, morphogens, motility, and methodology. Dev. Cell *21*, 2–4.

Little, S.C., Tkačik, G., Kneeland, T.B., Wieschaus, E.F., and Gregor, T. (2011). The formation of the Bicoid morphogen gradient requires protein movement from anteriorly localized mRNA. PLoS Biol. *9*, e1000596.

Liu, F., Morrison, A.H., and Gregor, T. (2013). Dynamic interpretation of maternal inputs by the *Drosophila* segmentation gene network. Proc. Natl. Acad. Sci. USA *110*, 6724–6729.

Maamar, H., Raj, A., and Dubnau, D. (2007). Noise in gene expression determines cell fate in *Bacillus subtilis*. Science *317*, 526–529.

Manu, Surkova, S., Spirov, A.V., Gursky, W., Janssens, H., Kim, A.R., Radulescu, O., Vanario-Alonso, C.E., Sharp, D.H., Samsonova, M., and Reinitz, J. (2009). Canalization of gene expression in the *Drosophila* blastoderm by gap gene cross regulation. PLoS Biol. *7*, e1000049.

Margolis, J.S., Borowsky, M.L., Steingrímsson, E., Shim, C.W., Lengyel, J.A., and Posakony, J.W. (1995). Posterior stripe expression of hunchback is driven from two promoters by a common enhancer element. Development *121*, 3067–3077.

Mirouze, N., Prepiak, P., and Dubnau, D. (2011). Fluctuations in spo0A transcription control rare developmental transitions in *Bacillus subtilis*. PLoS Genet. *7*, e1002048.

Munsky, B., Neuert, G., and van Oudenaarden, A. (2012). Using gene expression noise to understand gene regulation. Science *336*, 183–187.

Nachman, I., Regev, A., and Ramanathan, S. (2007). Dissecting timing variability in yeast meiosis. Cell *131*, 544–556.

Newman, J.R., Ghaemmaghami, S., Ihmels, J., Breslow, D.K., Noble, M., DeRisi, J.L., and Weissman, J.S. (2006). Single-cell proteomic analysis of *S. cerevisiae* reveals the architecture of biological noise. Nature *441*, 840–846.

O'Brien, T., and Lis, J.T. (1993). Rapid changes in *Drosophila* transcription after an instantaneous heat shock. Mol. Cell. Biol. *13*, 3456–3463.

Paré, A., Lemons, D., Kosman, D., Beaver, W., Freund, Y., and McGinnis, W. (2009). Visualization of individual Scr mRNAs during *Drosophila* embryogenesis yields evidence for transcriptional bursting. Curr. Biol. *19*, 2037–2042.

Perry, M.W., Bothma, J.P., Luu, R.D., and Levine, M. (2012). Precision of hunchback expression in the *Drosophila* embryo. Curr. Biol. *22*, 2247–2252.

Porcher, A., Abu-Arish, A., Huart, S., Roelens, B., Fradin, C., and Dostatni, N. (2010). The time to measure positional information: maternal hunchback is required for the synchrony of the Bicoid transcriptional response at the onset of zygotic transcription. Development *137*, 2795–2804.

Raj, A., Peskin, C.S., Tranchina, D., Vargas, D.Y., and Tyagi, S. (2006). Stochastic mRNA synthesis in mammalian cells. PLoS Biol. *4*, e309.

Raj, A., Rifkin, S.A., Andersen, E., and van Oudenaarden, A. (2010). Variability in gene expression underlies incomplete penetrance. Nature *463*, 913–918.

Rao, C.V., Wolf, D.M., and Arkin, A.P. (2002). Control, exploitation and tolerance of intracellular noise. Nature *420*, 231–237.

Raser, J.M., and O'Shea, E.K. (2005). Noise in gene expression: origins, consequences, and control. Science *309*, 2010–2013.

Reiter, M., Kirchner, B., Müller, H., Holzhauer, C., Mann, W., and Pfaffl, M.W. (2011). Quantification noise in single cell experiments. Nucleic Acids Res. *39*, e124.

Saffer, A.M., Kim, D.H., van Oudenaarden, A., and Horvitz, H.R. (2011). The *Caenorhabditis elegans* synthetic multivulva genes prevent ras pathway activation by tightly repressing global ectopic expression of lin-3 EGF. PLoS Genet. *7*, e1002418.

Sauer, F., Rivera-Pomar, R., Hoch, M., and Jäckle, H. (1996). Gene regulation in the *Drosophila* embryo. Philos. Trans. R. Soc. Lond. B Biol. Sci. *351*, 579–587.

Shermoen, A.W., and O'Farrell, P.H. (1991). Progression of the cell cycle through mitosis leads to abortion of nascent transcripts. Cell *67*, 303–310.

Sigal, A., Milo, R., Cohen, A., Geva-Zatorsky, N., Klein, Y., Liron, Y., Rosenfeld, N., Danon, T., Perzov, N., and Alon, U. (2006). Variability and memory of protein levels in human cells. Nature *444*, 643–646.

So, L.H., Ghosh, A., Zong, C., Sepúlveda, L.A., Segev, R., and Golding, I. (2011). General properties of transcriptional time series in *Escherichia coli*. Nat. Genet. *43*, 554–560.

Stewart-Ornstein, J., Weissman, J.S., and El-Samad, H. (2012). Cellular noise regulons underlie fluctuations in *Saccharomyces cerevisiae*. Mol. Cell *45*, 483–493.

Taniguchi, Y., Choi, P.J., Li, G.W., Chen, H., Babu, M., Hearn, J., Emili, A., and Xie, X.S. (2010). Quantifying *E. coli* proteome and transcriptome with single-molecule sensitivity in single cells. Science *329*, 533–538.

Tautz, D., Lehmann, R., Schnürch, H., Schuh, R., Seifert, E., Kienlin, A., Jones, K., and Jäckle, H. (1987). Finger protein of novel structure encoded by hunchback, a second member of the gap class of *Drosophila* segmentation genes. Nature *327*, 383–389.

Thummel, C.S., Burtis, K.C., and Hogness, D.S. (1990). Spatial and temporal patterns of E74 transcription during *Drosophila* development. Cell *61*, 101–111.

Treisman, J., and Desplan, C. (1989). The products of the *Drosophila* gap genes hunchback and Krüppel bind to the hunchback promoters. Nature *341*, 335–337.

Tsai, C., and Gergen, J.P. (1994). Gap gene properties of the pair-rule gene runt during *Drosophila* segmentation. Development *120*, 1671–1683.

Wilkie, G.S., Shermoen, A.W., O'Farrell, P.H., and Davis, I. (1999). Transcribed genes are localized according to chromosomal position within polarized *Drosophila* embryonic nuclei. Curr. Biol. *9*, 1263–1266.

Xu, T., and Rubin, G.M. (1993). Analysis of genetic mosaics in developing and adult *Drosophila* tissues. Development *117*, 1223–1237.

Zenklusen, D., Larson, D.R., and Singer, R.H. (2008). Single-RNA counting reveals alternative modes of gene expression in yeast. Nat. Struct. Mol. Biol. *15*, 1263–1271.

Cell

EXTENDED EXPERIMENTAL PROCEDURES

Total Transcript Content of Embryos by FISH

To estimate total maternal *hb* particle number during nuclear cycle 4, we obtained stacks spanning the distance from the embryo surface to the midsagittal plane, approximately 45 μm. For these samples, we obtained a count of particles (see below) from tiled stacks spanning the anterior-posterior axis. These values were then multiplied by 2 to account for imaging of one-half of the embryo to obtain a count of $7.4 \pm 1.9 * 10^5$ maternal particles per embryo (n = 4). In all cases, formaldehyde fixation, processing and mounting tended to reduce embryo length by approximately 10 to 15% and compression along the axis of imaging by about 25 to 30%; particle densities reported in absolute units are likely slightly lower in living embryos. Distortions introduced by the FISH procedure lead to approximately 3% inaccuracy in determining AP coordinates. Therefore, for simplicity we align embryos at the inflection point of spline fits when plotting values as a function of AP position from multiple embryos.

Absolute Quantitative RT-PCR in Single Embryos

Full-length *hb*-RB mRNA standard was synthesized from *Drosophila* melanogaster cDNA clone LD14196 (Berkeley *Drosophila* Genome Project) by digestion with ApaI and in vitro transcription using T3 mMessage mMachine (Life Technologies AM1348). mRNA integrity was assessed by denaturing mRNA agarose gel and concentration determined by absorbance at 260 nm. RT reactions were performed using Promega GoScript (A5000) and random primers, followed by qPCR with SYBR Green PCR master mix (Life Technologies 4309155) and primers against the *hb* open reading frame corresponding to the P1 promoter (forward primer: hbRB-F01, 5′- GAA TTG CAC TTG GAC TGT CCG CAA-3′, reverse primer: hbRB-R01, 5′- AAC ATG CTG TTG TAC CAG GCG TTG-3′) using an Eppendorf Mastercycler EP Realplex thermal cycler. Amplification efficiency with these primers was calculated by fitting a linear curve to $\log_2$(Ct) as a function of DNA plasmid template copy number (blue line in Figure S1H; copy number on x axis determined by spectrophotometry with error of 1.1%); the resulting line possessed slope of −0.98 with fitting error of ± 0.01 (note that in $\log_2$ plot, slope of −1 corresponds to perfect efficiency). We constructed an mRNA standard curve (red line in Figure S3) by single-parameter fit of a line of slope −0.98 to the *hb*-RB dilution series to obtain a y-intercept value with error of ± 0.4 cycle (1%). The error in the conversion of Ct to molecule number (3.1%) is found by summing the error in quantifying the mRNA standard by spectrophotometry with that of determining the amplification efficiency and that of determining the C-intercept. Individual embryos were collected between 30 and 60 min after egg deposition (AED), dechorionated in bleach, macerated under a dissecting stereomicroscope with a 26 gauge needle in 10 ul of Trizol (Life Technologies 15596-026), transferred to a 500 ul volume of Trizol, and RNA purified with RNeasy MinElute Cleanup kit (QIAGEN). Dilution series of individual embryos were obtained by 2-fold dilutions. Loss of mRNA was estimated by adding a known amount of in vitro transcribed *hb*-RB mRNA to Trizol followed by purification and comparing the Ct to that obtained by adding the same amount of mRNA directly to the RT reaction. The variation in counts from embryos (36%) is similar to that introduced by the purification protocol itself (31%).

α-Amanitin Injection

a-amanitin was injected at a concentration of 1 mg/ml at about 90 ± 8 min after egg deposition as previously described (Edgar et al., 1986). Batches of 10 embryos were collected and processed for RT-qPCR as above except that oligo-dT primers were used for reverse transcription. For each batch of embryos, Ct values were found for the zygotic *hb*-RA transcript and for *tubulin56D* with three technical replicates. Values plotted in Figures S3E and S3F are relative expression levels calculated as $2^{\wedge}(Ct_{hb} - Ct_{tub})$. Primer sequences: hbP2-fwd: 5′- CGG CCA CGA AAC GCC GTC TAG −3′, hbP2-rev: 5′- CCA GGC GTT GTG CTG CTC GTA −3′, Tub56D-fwd: 5′- GGC GCC AAG TTC TGG GAG ATC ATC T −3′, Tub56D-rev: 5′- TCG CTG TCA CCG TGG TAG GCG −3′.

FISH Image Analysis

A single entry in our data set library contains the following set of objects:

- Two low-magnification DAPI images of the whole embryo in register with each other: one in the midsagittal plane and one at the surface;
- A high-magnification DAPI image of the surface of the embryo in register with the FISH channel(s);
- One or more channels of FISH data, each containing a flat-field image and a confocal stack of images;
- A "tag file" containing all the information describing the embryo and the channels.

To achieve dynamic range required for an accurate measurement of spots as dim as single cytoplasmic transcripts and as bright as sites of nascent transcription, we acquire two FISH stacks for each fluorophore color: a low-power stack for measuring transcription intensity, followed by a high-power stack for measuring cytoplasmic counts. For experiments that did not include transcription intensity measurements, only high-power stacks are collected for each gene of interest.

Image analysis can be split into five major steps:

1. Preprocessing of image stacks and collection of information on the embryo
2. Identifying fluorescent particles
3. Defining summation volumes for cytoplasmic counts and transcription sites

4. Calibrating total fluorescence to measure transcription intensity and cytoplasmic counts
5. Extracting features of cytoplasmic profiles

Preprocessing of Image Stacks

Raw image stack is flat-field corrected and realigned (up to 2 pixel xy shift between individual frames) to compensate for stage drift. Alignment shifts are determined by maximizing cross-correlation between central 300-by-300 pixel regions of successive frames. Low-magnification midsagittal DAPI image is thresholded to obtain the embryo mask. The points of the embryo that extend the furthest along the major axis of this ellipsoid-like mask are designated as ends of the antero-posterior axis (the embryo is always imaged in the same orientation, allowing the software to correctly select the anterior and posterior tips). High-magnification DAPI image is resized to the same scale as low-magnification DAPI image of the embryo surface and correlation analysis (search for xy location providing the best match between two images) is used to identify the exact location of the high-magnification imaged region within the embryo.

Next, high-magnification DAPI image of the embryo surface is used to identify the locations of nuclei centers. Detection is performed by an automatic routine and is verified and corrected by human input, particularly for embryos in mitosis where, by convention, one nuclear center is selected for each dividing nucleus. This resolves any ambiguity in cases where the embryo was fixed in the middle of a mitotic wave.

Finally, we manually select a region along the midline of the embryo (at least 5 nuclei wide in nc12, and at least 20 nuclei wide in nc14) where tissue deformation, which can be visually estimated via the change in density of nuclei, is minimally inhomogeneous. Cytoplasmic counts are measured in fixed physical volumes and so are affected by the degree of tissue compression; we therefore only measure them in nuclei belonging to this minimally deformed ''center band.'' In contrast, our measure of total transcription activity of a nucleus is insensitive to tissue deformation, so we use all nuclei to improve statistics. Using only nuclei in the center band does not reduce the measured noise of transcription activity.

Identifying Fluorescent Particles

Raw images are filtered using a Difference-of-Gaussians (DoG) filter with inner and outer Gaussian parameters 1.2 and 2.2 pixels, respectively. This is a balanced filter giving a measure of local contrast (zero response on a constant image and high response on a spot, i.e., a locally bright region surrounded by a dark one). A ''master threshold'' is chosen (in a manner that will be described shortly) and local maxima exceeding this threshold in the DoG-filtered images are detected in each frame individually. This yields a list of several million ''bright spots,'' on the order of 30 thousand per frame. Given that the step in z direction in our confocal stacks is several times smaller than the width of the PSF of the microscope (Figure S1D), each true point-like source of fluorescence is clearly visible at the same location on at least 3 consecutive slices. We call these multiple images of the same real particle ''shadows'' of each other. In contrast, random fluctuations in the background are extremely unlikely to happen at the same position in two independent frames. This provides a powerful filtering criterion: we arrange all detected bright spots into columns of ''shadows'' (allowing a $\pm$ 2 pixel relative shift in xy position to account for a possible shift due to imaging noise or physical movement) and reject all columns of height less than 3. All columns with two clear peaks in z are separated; finally, the brightest shadow in each column is identified as a candidate true particle. This selection process eliminates $>$ 90% of bright spots and allows us to obtain remarkable signal-noise separation (Figure 1D). Reducing the required number of shadows to 2 increases the total number of detected particles by $<$ 3% percent.

The master threshold is adjusted iteratively so that in the end, the particle intensity histogram (Figure 1D) exhibits two peaks of equal heights when plotted on linear intensity scale: the peak of spots due to random imaging noise and the peak of cytoplasmic mRNA. This ensures that the master threshold is low enough that even the dimmest cytoplasmic particles had all 3 shadows detected, but not too low so as to lead to an explosion of noise peak (the shadow filtering scheme breaks down if local maxima are detected at a density where spontaneous creation of columns is ubiquitous). A bleaching factor (typically $\sim$5% intensity loss per 10 frames) is determined from a linear fit of logarithm of particle intensity versus index of frame, and raw intensities of frames are bleach-corrected accordingly. After correction, intensity distributions of detected particles coincide for all depths.

This entire analysis step, including threshold choice, is fully automated.

Defining Summation Volumes for Cytoplasmic Counts and Transcription Sites

We begin by labeling all candidate particles as transcription sites, cytoplasmic transcripts or noise. The labeling is performed using simple global thresholding of bleaching-corrected particle intensity. The threshold separating cytoplasmic transcripts from noise is defined as the bottom of the valley between the two peaks on the particle intensity distribution histogram as on Figure 1D (red line). The threshold between cytoplasmic transcripts and transcription sites (Figure 1D, green line) is determined from the observation that unlike cytoplasmic particles, transcription sites are tightly clustered in z. We list candidate particles in order of decreasing intensity and construct a running SD of their z coordinate in a window of 50 particles. We observe a sharp transition between ''tightly clustered'' and ''equally likely to appear at all depths''; and use it to set the threshold. Both threshold-setting procedures are automatic; the latter is approved by human input and corrected if necessary, e.g., in embryos undergoing mitosis where no transcription sites are visible by eye nor expected to be present. Typical transcription site threshold intensity set in this manner is 3-4 times the mean intensity of a cytoplasmic particle. A flexible threshold outperforms a fixed one (a constant number of cyto units in each embryo), because the optimal threshold is lower in younger embryos (with fewer cyto spots) than in older embryos, where a large number of cytoplasmic transcripts makes them more likely to randomly exceed the same threshold.

Particles identified as transcription sites are each enclosed in a parallelepiped of 19 × 19 × 9 pixels (1.4 × 1.4 × 2.3 μm^3); total fluorescence collected from these volumes is attributed to transcription activity, and assigned to nuclei using a Voronoi tessellation based on nuclear centers. The choice of parallelepipeds rather than cylinders was motivated by computational efficiency; all total fluorescence-based measurement are background corrected (see below) and were checked not to depend on the choice of shape of summation volume for transcription sites.

For cytoplasmic mRNA, we defined a measure of local expression based on the number of transcripts contained in a band of 12 μm from the plasma membrane. This choice was motivated as follows. On the one hand, we would like our measure to be local, reflecting the transcriptional output of an individual nucleus, inasmuch as it is possible in a syncytium. On the other hand, transcripts are largely depleted from nuclei during the majority of interphase (Figure 1E) and as nuclei change size, their spatial distribution varies accordingly; in nuclear cycle 14, as nuclei elongate, this spatial reorganization can extend up to a depth of 11-12 μm. Counting all transcripts within a band of 12 μm is therefore a natural compromise between keeping the summation volume small and reducing sensitivity to spatial reorganization of RNA density, focusing on transcript accumulation with age.

Specifically, we enclose each nucleus in a cylinder extending from the embryo surface down to 12 μm from the plasma membrane, centered at the nucleus center and of a diameter equal to the average internuclear distance in the "center band" of the embryo as defined above. We then exclude from this volume the parallelepipeds containing transcription sites, and define "mRNA count per nucleus" as the total number of transcripts in this volume, called summation cylinder. Note that, for consistency, we exclude transcription site parallelepipeds from cytoplasmic summation volume even when measuring direct counts of cytoplasmic particles (not based on total fluorescence). Since mRNA transcripts are largely excluded from nuclei, this modification of summation volumes changes the direct counts by less than 1%.

We stress that summing these numbers for all nuclei does *not* correspond to the total number of mRNA in the embryo; our goal is not to account for all mRNA molecules, but to quantify noise in transcription activity and output. For the same reason, we measure mRNA counts in cylinders of fixed volumes rather than a Voronoi-type tessellation of the embryo surface.

Note that the volume of the summation cylinder changes with age and decreases 2-fold with every nuclear division. To compare transcript density between embryos of different ages, we define "standard volume" as the volume of the summation cylinder at nuclear cycle 14, and rescale measured "counts per nucleus" into counts per standard volume, which we also call "counts per cell": for an embryo in nuclear cycle k, we define $N_{cell} = N_{nucleus}/2^{14-k}$. This quantity measures the number of transcripts in equivalent volumes and is directly comparable for embryos of different ages. The name "counts per cell" reflects the fact that at 14th nuclear cycle the embryo exits syncytial stage and cellularization occurs.

Calibrating Total Fluorescence

Measurements of cytoplasmic concentration in dense regions and of transcription activity are based on total fluorescence. To convert these to "cyto units," we use the following calibration procedure. A large number of test summation volumes are placed at regularly spaced positions within the center band in the embryo and transcription sites are excluded as described above (this allows us to obtain good statistics, since relation between total fluorescence and direct counts holds for any volume, and we need not be limited by the number of nuclei we sample). For each summation volume, we calculate the total fluorescence collected from it as well as its total volume in voxels. The former is tightly correlated with direct counts measured in the same volumes (see Figure S2A), and in a broad range of particle densities is well described by a linear dependence. For data in this linear regime (whose bounds are selected manually), we fit a two-parameter model: $F = \alpha D + \beta V$, where *(F, D, V)* is the data (total collected fluorescence, direct particle count and volume in voxels, respectively, for each summation volume), and the two parameters are α, total fluorescence of a single transcript, and β, background fluorescence per voxel. We call α "the cytoplasmic unit of total fluorescence," or "cyto unit" for short. Note that the explanatory fit on Figure S2A was plotted as if summation volumes were all identical; in practice this is true only approximately. This assumption was made only for clarity of presentation, and the analysis software performs the fit taking into account the (almost negligible) differences in volume. Knowing α and β, we can calculate "total fluorescence-based counts" C_F of mRNA per nucleus: $C_F = (F-\beta V)/\alpha$. The same formula allows converting total transcriptional intensity per nucleus into activity expressed in cyto units.

Finally, cytoplasmic counts are corrected for tissue deformation estimated using nuclear density fluctuations. For each nucleus the correction factor is determined as the square of mean internuclear distance to local internuclear distance, defined as the average distance to six nearest neighbors.

"Intensity" of a cytoplasmic particle always means DoG intensity (Figures 1D, 1F, and S1E–S1G). Total fluorescence is always measured in raw pixel values (Figure S2A; all transcription intensity measurements). Note that Figure 1F uses a "cyto unit of *intensity*," i.e., the mean DoG intensity of cytoplasmic particles. In all other cases "cyto unit" refers to the parameter α as defined above ("cyto unit of *total fluorescence*").

Extracting Features of Cytoplasmic Profiles

For each data set, the diagnostic plot as on Figure S2A is inspected to determine whether total fluorescence based counts or direct counts provide a better estimate of the expression in the "fully on" region. In young embryos (e.g., most nc12 embryos), cytoplasmic densities are low enough that the coordinated deviation from linearity is imperceptible, i.e., negligible compared to the spread of data points in the direction perpendicular to the roughly linear global trend. In these embryos, using total fluorescence would not change the mean level of cytoplasmic counts in any given bin along antero-posterior embryo axis, but would add noise. Consequently, for these embryos direct counts are used as more reliable; in cases such as depicted on Figure S2A, total fluorescence counts are used

instead. For every embryo the more reliable measure of cytoplasmic counts per nucleus is denoted *N*, and the plot of *N* versus normalized nuclear locations along antero-posterior axis (x/L) constitutes the "cytoplasmic profile." For every profile, its region of maximal expression is selected manually as a band of 5%–10% embryo length for *hb* and *gt*, and 4%–7% embryo length for *Kr* and *kni*. The mean cytoplasmic expression level within the maximal expression domain is denoted N^{max}. For every profile, a smoothed profile is obtained using a global cubic spline fit, constrained to zero derivative at the edges of the imaged region, with up to 4 internal breakpoints whose positions are adjusted to minimize χ^2; the number of breakpoints is a function of embryo age and reflects the fact that profile shape becomes more complex with time (Figure S3C). Expression noise is defined as the root-mean-square deviation of data points from the smoothed profile in the region of maximal expression.

Control Experiment Demonstrating Single-Molecule Resolution

Embryos in nuclear cycles 11-13 were processed with a set of FISH probes against *hb* mRNA, conjugated to fluorophores whose colors alternated along the transcript length. For cytoplasmic particles that were independently detected in both channels, we constructed a two-dimensional histogram of their intensities as detected using both colors (Figure 1F). If all cytoplasmic particles corresponded to a single mRNA transcript, the distribution of red (r) and green (g) particle intensities, expressed in cyto units, would be a two-dimensional Gaussian $G_1(r, g)$ centered at (1,1), since probes conjugated to red and green fluorophores target different binding sites and binding events are, to a good approximation, independent. In practice, red and green measurements exhibit a weak correlation (Figure 1F), which can be due to several reasons, one of which is correlation through mRNA content. Let $p(n)$ be the probability for a given particle to contain n mRNA transcripts, then if we attribute all of the observed correlation on Figure 1F to this source of correlation, we find that the intensity distribution function G(r, g) is given by a convolution of $G_1(r, g)$ with $F(r,g) = \sum_n p(n)\delta(r-n)\delta(g-n)$. Since variances add under convolution, the variance of $p(n)$ can be found as the difference between the variance of the cross-section of G(r, g) along the correlated direction (line r = g) and the variance of $G_1(r, g)$ which, in turn, is equal to the variance of G(r, g) along the anticorrelated direction (line r = 2-g).

We thus find an upper bound of 16% on the fractional standard deviation of $p(n)$. In an independent measurement using RT-qPCR (below), we show that an embryo contains, on average, 1.2 ± 0.5 mRNA molecules per observed cytoplasmic particle. This constrains the mean of $p(n)$, and notwithstanding the large error bar due to imprecision of RT-qPCR, we can conclude that $p(n)$ is concentrated on n = 1 and n = 2, with higher contributions being negligible. The result $\sigma[p(n)] < 16\%$ becomes highly constraining: denote $p = p(1)$, then $\sigma/\mu = \sqrt{p(1-p)}/[p+2\times(1-p)] = 0.16$, which entails p = 0.97, or 97% of observed spots are single molecules.

Noise Level Predicted by the Two-State Model of Transcription

At saturation of transcription factor concentration, the two-state model of transcription (Figure S4C) reduces to a single-step description of transcription initiation. To a first approximation, this predicts a Poisson-distributed number of initiation events in a given time window. Using probes distributed evenly along the length of the mRNA, a mean transcriptional activity of about 50 C.U. in total nascent mRNA content (Figure 3D) corresponds to 100 uniformly distributed RNAP across all loci. This is in agreement with a lower bound of a cytoplasmic accumulation rate of at least 500 transcripts during the 15 min of interphase nc13 (Figure 2B), indicating a minimum of 33 transcripts made by each nucleus per minute. Consistent with previous estimates of RNAP processivity (Shermoen and O'Farrell, 1991) and with our measurements of mRNA lifetime, this requires at least $(33/\text{min}\times 3.2\text{kbp})/(1.4\text{kbp min}^{-1}) = 80$ engaged RNAP at a given instant. If RNAP numbers fluctuate according to a Poisson distribution: the predicted fractional error should be at most $\sqrt{80}/80 \cong 11\%$. As noted, the actual mean number of RNAP is higher than 80 per nucleus, but larger numbers even further lower the expected noise.

However, if the initiation rate is large enough that the density of bound RNAPs becomes comparable to the maximum attainable density of polymerases, the assumption of independent binding is no longer valid: there is a minimum time delay that must separate consecutive binding events, since the next RNAP can only bind after the previous one has cleared the landing site (RNAP crowding). To numerically study the consequence of this effect on the statistics of binding events, we performed Gillespie simulation of RNAP binding in various parameter regimes. (Note that the simulation has only two parameters, the mean output rate and the minimum time delay between binding events, and the first is fixed by our measurements.) We find that, in general, RNAP crowding effect leads to a mild reduction of output noise. This can be intuitively understood as follows: at density close to maximal, the polymerases are forced to "walk" in tight synchrony, since no polymerase can overtake another. In the limit of low density, crowding becomes irrelevant and we obtain the simple Poisson regime. As we report in this work, for gap gene transcription, the average RNAP density is low enough to allow large (~50%) fluctuations of polymerase load of individual sites. One would not, therefore, expect RNAP crowding to play a significant role, and indeed, simulations show that for RNAP exclusion footprint of 50–80 bp, the reduction in noise level compared to Poisson statistics is from 11% (Poisson prediction) to 10%.

Efficiency of Temporal and Spatial Averaging

The RNAP processivity of 1.1–1.4 kbp/minute (Irvine et al., 1991; Shermoen and O'Farrell, 1991; Thummel et al., 1990) corresponds to a minimum time of 2.3 min for an RNAP to traverse the 3.2 kbp of the *hb* gene (the RNAP "correlation time"). A reasonable estimate of the time available for transcription during the thirteenth interphase is 15 min, i.e., this is the available "integration time" over which accumulation of transcripts may occur. With these values, noise reduction by temporal averaging alone may be estimated as $\sqrt{15/2.3}$, or a factor of ~2.6. The number of accumulated transcripts produced from one nucleus during nc13 can be found using

starting and ending *hb* counts of approximately 400 ± 30 and 1,000 ± 70; the noise in production is therefore $\sqrt{70^2 - 30^2} = 63$. Thus, the precision in production of $63/100 \approx 11\%$ is similar to the reduction in nascent transcript noise by 2.6-fold, from 22% to about 9%. Therefore, according to this estimate, temporal averaging can easily provide the required noise filtering by allowing stable mRNA to accumulate while RNAP numbers fluctuate during the course of interphase.

A more careful estimate (see Figure S6B), however, allows to obtain a theoretical bound on the maximum efficiency of temporal averaging based on the quantities we measure directly. In the case of *Kr* mRNA profile, it shows that by the time the mean expression level reaches 800 molecules per nucleus, pure temporal averaging can at most reduce the expression noise to 8%. For these late embryos, however, our measurements show a consistently lower noise level of 6% ± 2%. This subtle discrepancy can be accounted for by spatial averaging.

Let p be the probability that an mRNA produced by one nucleus is found within the volume assigned to a particular neighboring nucleus. In a hexagonal lattice, the total fraction of exchanged transcripts is $6p$. Considering that all exchange events are independent (and so the variances add), we find that spatial averaging reduces noise level σ to $\sqrt{(1-6p)^2\sigma^2 + 6(p\sigma)^2} \equiv \sigma/\chi$, where χ denotes the fold reduction in noise. The observed excess filtering compared to what can be achieved by temporal averaging corresponds to $\chi = 8\%/6\% = 1.3$. Solving for p, we find p = 0.04, which corresponds to just 32 transcripts exchanged between neighboring volumes during the entire development time during which 800 transcripts per nucleus were produced. Thus, even a limited degree of spatial averaging is completely sufficient to account for the appearance of low variation in cytoplasmic accumulation from stochastic transcription.

Transcriptional Activity of Loci on Sister Chromatids

Pairs of loci representing sister chromatids were selected automatically in n = 4 embryos, heterozygous for deficiency in *hb* (and consequently possessing at most two transcription sites per nucleus). The selection criterion was for the pair of spots to exceed a manually selected brightness threshold and be detected at least 4 pixels apart while still belonging to the same nucleus. The brightness threshold was chosen conservatively to exclude any possibility that a single cytoplasmic transcript could be mistaken for a transcription site. Automatically selected pairs were manually inspected for misdetections. Transcriptional activities of the two loci were measured using the difference-of-Gaussian intensity estimator (DoG) that is linearly related to the nascent mRNA content. The slope and offset of this linear relation are hard to estimate precisely (and so, when measuring transcriptional activity per nucleus, we use total fluorescence instead of the DoG estimator); however, correlation between variables are preserved by linear transformations, and consequently, the analysis of correlation between the activities of sister loci can be performed directly on DoG values (Figure 4B). As a control, we used n = 4 embryos labeled using *hb* probes of alternating colors and compared the DoG intensities of all transcription sites that were detected in both channels. The tight correlation (Figure 4D) demonstrates that the lack of correlation on Figure 4C cannot be attributed to the intrinsic noisiness of the DoG estimator itself, and indicates that the transcriptional activities of sister chromatids are indeed uncorrelated.

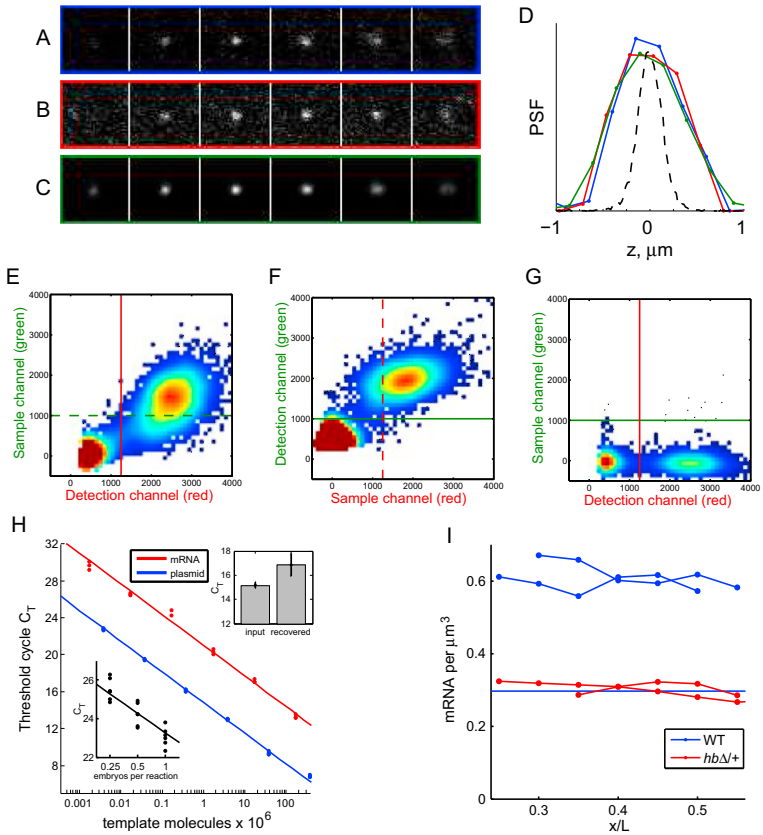

Figure S1. Detection of Individual *hb* Transcripts, Related to Figure 1

(A–D) 3d detection and point spread function. Fluorescent particles appear on 6 consecutive confocal slices spaced by 250 nm. A cytoplasmic mRNA transcript (A), a nascent transcription site (B), and a fluorescent bead (C) are shown in 42 × 42 pixel windows; pixel size is 76 nm. (D) Axial intensity profiles (point-spread-functions in z) for particles in (A, blue), (B, red) and (C, green), normalized to unit integral. For comparison, lateral intensity profile versus x is shown on the same axis (black dashed line; normalization scaled to fit axis).

(E–G) Particle detection efficiency. After labeling mRNA with alternating colors, thresholds were found for each channel as in Figure 1D. Because a particle may be detected at two different positions in each channel (typically ± 1 pixel, either from imaging noise or physical movement of the sample), we choose one channel for detection and measure intensity in the other (sample). This procedure therefore provides a lower bound on detection efficiency. Plots show 2d intensity histogram for all detected spots.

(E) 2d histogram showing green intensity at the exact locations of red particles versus their red intensities. Distribution is clearly bimodal in 2d, demonstrating good colocalization. Red and green lines indicate thresholds for each channel. Of red spots classified as mRNA particles, at most 22% escape detection in green channel (are classified as "noise").

(F) Same as E, but with detection and sample channel inverted. Of red spots classified as mRNA particles, at most 27% escape detection in green channel. The probability for an mRNA molecule to go undetected in both channels is therefore at most 0.22 ⋆ 0.27 = 6%, i.e., the detection efficiency is better than 94%.

(G) As a control, we repeat the procedure in (E), but plot green intensities not at the exact locations of red particles, but shifted by 5 pixels (0.38 μm) in both x and y. The high degree of correlation (i.e., color colocalization) exhibited on (E) is lost.

(H) Absolute RT-qPCR control measurement. Threshold cycle Ct as a function of number of plasmid DNA (blue) or in vitro synthesized *hb* mRNA (red) molecules per PCR with (for mRNA) or without (for plasmid) reverse transcription. Nucleic acid concentration was determined by spectrophotometry with a measurement error of 1.1%. Ct for each amount of nucleic acid was assayed in 4 independent reactions. Lower inset: Ct for individual embryos 30-60 min in age processed and diluted as described in Experimental Procedures (n = 6 whole embryos, n = 6 embryos serially diluted). Linear fits to data and error propagation were performed as described in Extended Experimental Procedures. Upper inset: the mean and SD in Ct when 2.4 ⋆ 10^7 molecules of standard mRNA were analyzed by RT-qPCR either by adding directly to the reaction (input, 4 independent samples) or after processing with same RNA extraction protocol used for embryos (recovered, n = 10 independently processed samples). Using mRNA standard curve to convert Ct to mRNA number, the extraction protocol yields recovery of 0.77 ⋆ 10^7/2.4 ⋆ 10^7 = 32% of input, and increases the measurement variability (fractional SD) to 31%, compared to 12% without the extraction protocol. By RT-qPCR, an Ore-R embryo contains 8.7 ± 3.1 ⋆ 10^5 mRNAs.

(I) Maternal *hb* mRNA density in *hb*Δ/+ and WT embryos differs 2-fold. Density (molecules per μm^3) of maternal *hb* mRNA as a function of position along the AP axis. Data shown for two WT embryos (blue traces, both in nc8), and two *hb*Δ/+ embryos (nc7 and 8). Solid blue line is at half the mean of WT traces. Density was measured by counting all transcripts in a band running along the center of the embryo of width equal to 30% egg length (EL), in a stack of 20 frames (5 μm in z), binned in regions 5% EL wide. These volumes contain about 4500 maternal mRNA molecules in a WT embryo.

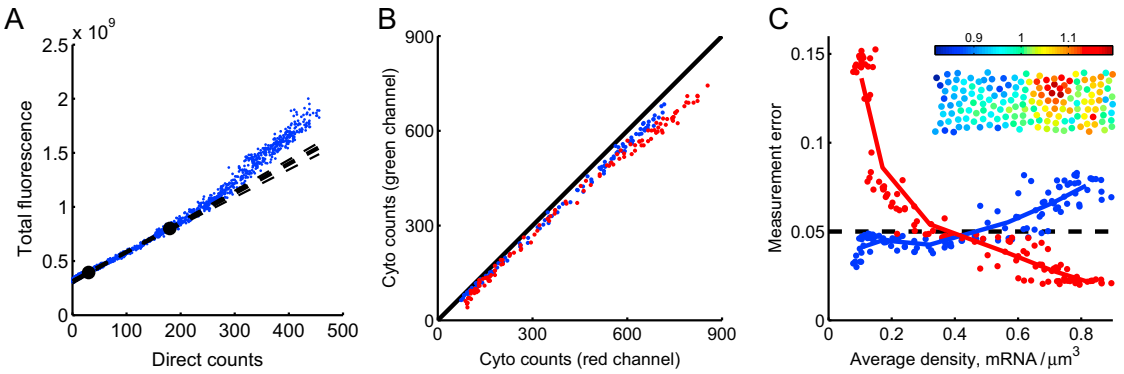

Figure S2. Particle Counts and Total Fluorescence, Related to Figure 1

(A) Correction factor for densely populated regions. The total fluorescence of labeled cytoplasmic *hb* mRNA is shown as a function of number of resolved particles ("direct counts") in the same averaging volume. The deviation from a linear dependence at high counts occurs when spots become too dense to be resolved reliably, at approximately 1 molecule per μm^3. Each data point corresponds to a summation volume of $2.8 * 10^5$ $pixel^3$, i.e., 400 μm^3 (cylinders with radius ~3 μm and height 13 μm drawn at regular intervals from a band parallel to AP axis). Bold dashed line is a fit to the data between manually selected black dots; its slope is the total fluorescence collected per mRNA molecule ($2.7 * 10^6$ pixel intensity units) and its offset is background fluorescence ($\sim 1.1 * 10^3$ pixel intensity units per voxel). These parameters provide absolute calibration to convert total fluorescence into absolute mRNA number in high density regions. Error bars of the fit (light dashed lines) are 12%; this includes the uncertainty arising from the choice of the range used for the linear fit (location of the black dots). This 12% error defines the uncertainty in absolute measurement of cytoplasmic concentration in dense regions.

(B and C) Precision of total fluorescence measurements and of direct counts as a function of mRNA density. Cytoplasmic counts of *hb* mRNA were measured using probes of alternating colors, using direct particle counts or calibrated total fluorescence in each of the two color channels.

(B) Scatter plot of cytoplasmic counts per nucleus as measured in red and green channels (direct particle counts, blue; calibrated total fluorescence, red). The error of *absolute* concentration measurement is 10% for direct counts and 12% for total fluorescence counts, determined as deviation from 1:1 slope. This error is dominated by uncertainty of intensity threshold selection when assigning direct counts, and by the normalization procedures when calibrating total fluorescence.

(C) Precision of *relative* measurements made using direct particle counts (blue) or calibrated total fluorescence (red), as a function of average (not peak) mRNA density in summation volume. Error is defined as the root-mean-square deviation of data points from the linear slope in (B), scaled by the mean (distance to [0, 0]). As expected, direct counts (total fluorescence) are more precise at low (high) densities, respectively. Overall the precision of relative measurements of cytoplasmic counts *in a given volume* is 5% (dashed line); in the region of maximal expression it goes down to 2%–3%. Inset: The uncertainly of expression noise measurement is dominated not by uncertainly of counting, but by the uncertainty in summation volume definition arising from tissue deformation after hybridization. Shown are nuclei in a stripe along the midline of an embryo, color-coded to highlight inhomogeneity of nuclear density in fixed samples. Color indicates density (number of nuclei per unit area) relative to the average density; this is used as a correction factor for cytoplasmic counts to compensate for tissue deformation. Absolute magnitude of correction can reach 15% in deformed embryos (as shown); local fluctuations of correction factor (imperfect compensation) are 5% and dominate the uncertainty in measuring expression noise (compare with 2%–3% of counting uncertainty in a given volume).

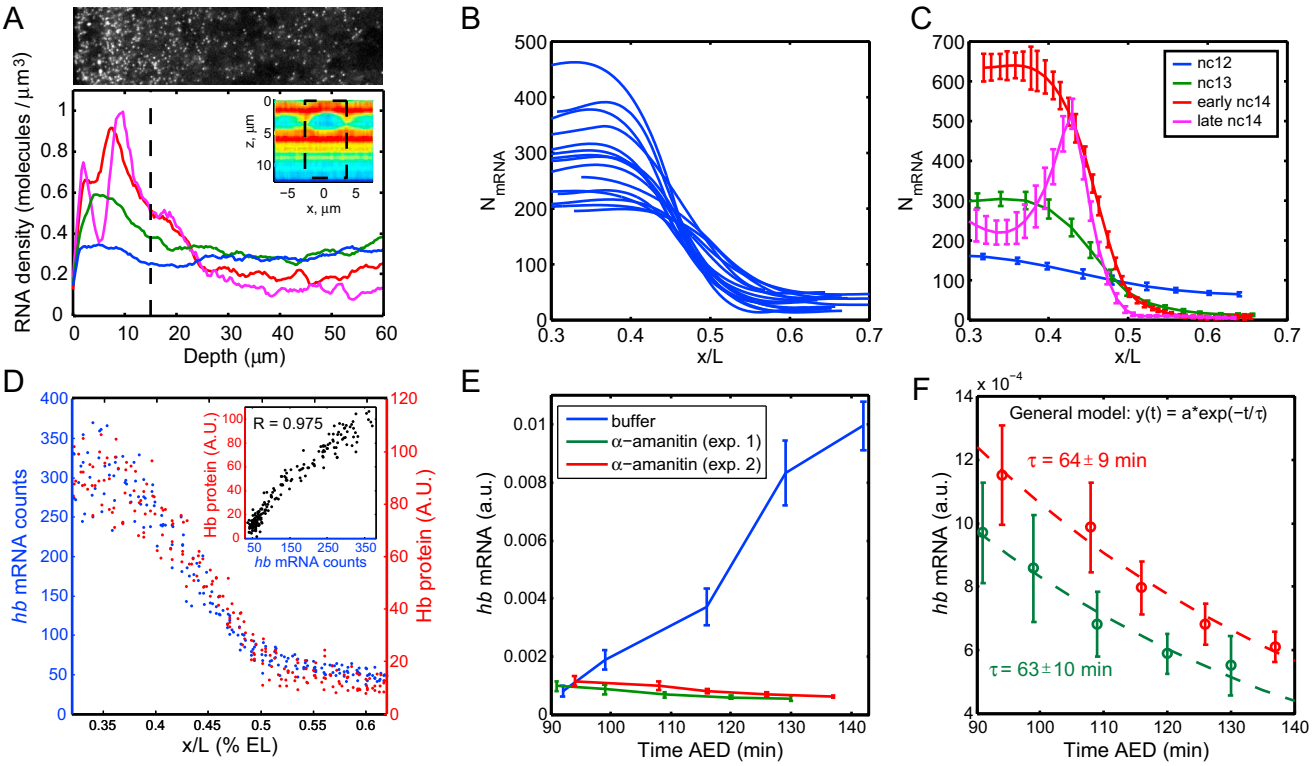

Figure S3. Spatial Distribution of *hb* mRNA, Comparison to Hb Protein, and *hb* mRNA Lifetime Measurement, Related to Figure 2

(A) Upper: midsagittal view of a 1 μm projection of a 15 μm × 60 μm stripe of an nc14 embryo labeled with *hb* probes. Lower: Average particle density was computed over a stack of 20 slices in a window of 15% EL in AP width for 4 embryos in nuclear cycle 12 (blue), 13 (green), early 14 (red) and late 14 (magenta). Dotted line shows an approximate depth of summation cylinders we use for our measure of local mRNA output: we use 12 μm from the surface in flattened (compressed) embryos, which roughly corresponds to 15 μm in the uncompressed midsagittal plane used for this figure; the compression factor is determined from the aspect ratio of the imaged nuclei that, up to early nc14, are approximately spherical prior to mounting. Figure 1E is shown for comparison (inset). Apical spot density depends on the exact structure of nuclear layer and therefore on age within interphase (compare red and magenta traces). Setting the threshold at 12 μm we eliminate this source of variation and obtain a measure of total expression that is largely insensitive to spatial reorganization of mRNA. A resulting source of error due to uncertainty of z-positioning (detection of embryo surface and the varying degree of embryo deformation) can be estimated from this depth distribution to 5% per μm of z-error (i.e., for these embryos, if the threshold is set at 13 μm instead of at 12 μm, 5% more spots would be counted). This is the single largest source of error in data points on Figure 6.

(B) Cytoplasmic *hb* mRNA profiles for 15 embryos during interphase 13 (counts per standard volume versus position along AP axis). Smooth profiles were obtained using spline fits; individual data points (data not shown) follow these profiles with 8% ± 2% root-mean-square deviation.

(C) Cytoplasmic *hb* mRNA profiles of Figure 2A plotted versus absolute AP position rather than relative, showing smoothed profiles during interphase 12 (blue), 13 (green), 14 early (red) and 14 late (magenta). Lines are best spline fits with 1, 2, 3 and 4 internal breakpoints, respectively. Error bars are root-mean-square deviations from smoothed profile, calculated in windows of 10 nuclei.

(D) Profiles of *hb* mRNA and Hb protein in an embryo simultaneously processed for FISH and immunofluorescence show a strong correlation (Spearman's correlation coefficient R = 0.975). Note that dual labeling significantly impairs quantification performance.

(E) Amount of zygotically expressed *hb* mRNA as a function of time after egg deposition (AED) as determined by RT-qPCR relative to *tubulin56D* at various times after injection of embryos with α-amanitin (two separate experiments, green and red lines) or buffer only (blue line). First time point at ~92 min corresponds to injection time. Error bars are SDs across technical replicates.

(F) Results of two independent injection experiments were fit to a model of exponential decay to yield a *hb* mRNA lifetime τ of about 60 min (mean and SD indicated in figure are from nonlinear least-squares fits using a restricted step method).

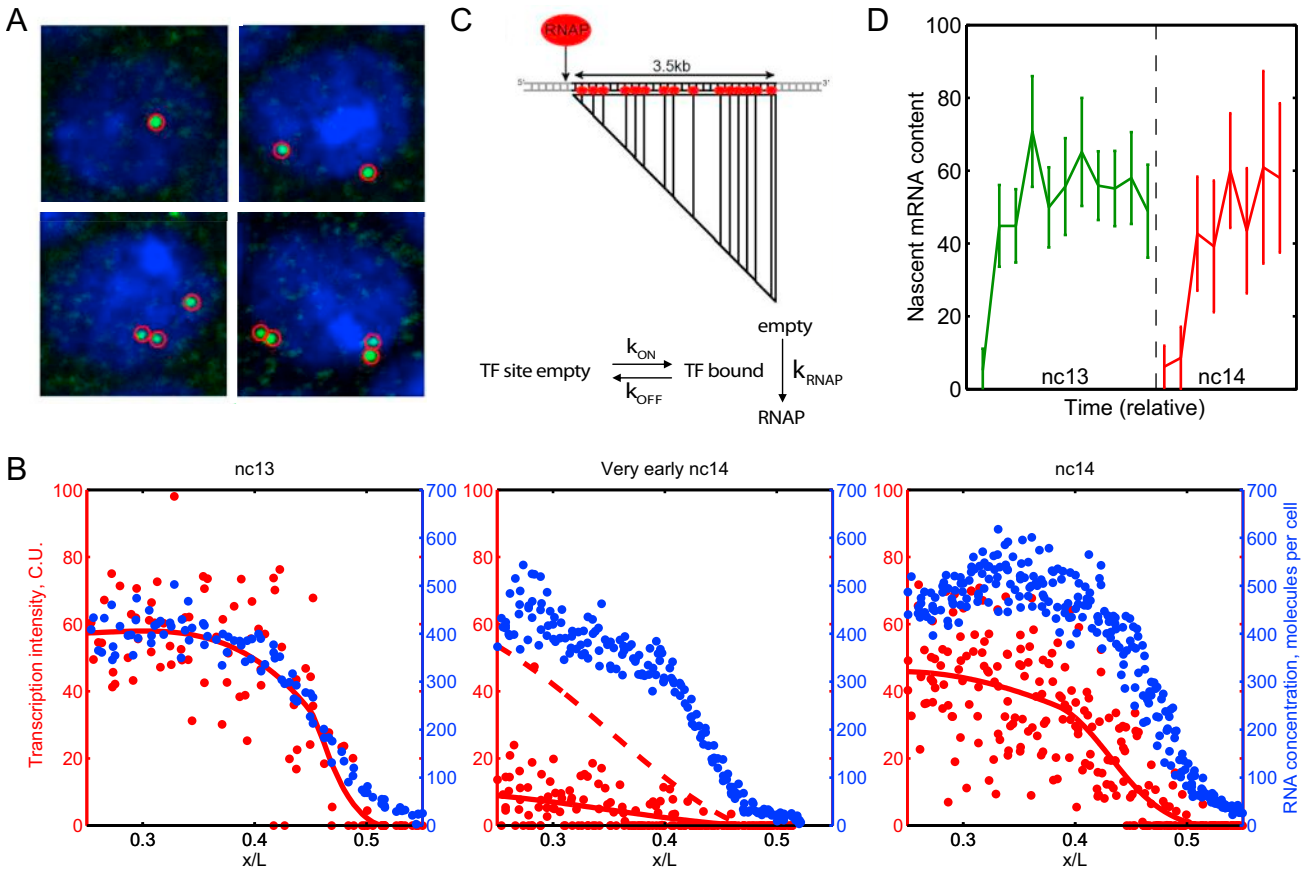

Figure S4. Detection and Interpretation of Transcription Dynamics, Related to Figure 3

(A) An overlay of *hb* FISH data showing active sites of nascent transcription (green) and DAPI staining of DNA (blue) for four nuclei in a single embryo at interphase 13. Red circles indicate active transcription sites. Up to four transcription sites can be distinguished; however, resolving sister chromatids is only possible if they are well-separated and if this separation occurs in the lateral plane (due to impaired confocal resolution in the axial-direction; see Figure S1D).

(B) Transcriptional activity per nucleus in cyto units (red) and cytoplasmic mRNA counts per standard volume (blue) for embryos of three similar ages: late interphase 13 (left), first minute of interphase 14 (middle), and early interphase 14 (right). Smoothed profiles are depicted as solid red lines. During interphase, the shape of transcription activity profile is very similar to that of cytoplasmic mRNA concentration (left and right). However, in approximately the first minute after completion of mitosis, anterior nuclei activate *hb* earlier than those located more posterior (middle). If the nascent mRNA content of active loci is dominated by the loading and progression of RNA polymerases along the length of the genomic template, then in the first minute of interphase we expect the nuclei located in the domain of maximal expression to exhibit a gradient of mean transcription activity, as indeed observed (middle). Red dashed line is the smoothed transcription profile multiplied by an arbitrary factor of 5 so as to visually highlight its distinction from the step-like shape observed on the other panels. Note the presence of transcriptionally silent nuclei along the entire length of AP axis on the middle panel. Their presence is a signature of a very early postmitotic stage. Rare in the very anterior and more and more abundant toward the posterior, these nuclei shape the gradient of the averaged profile.

(C) In the simplest description of initiation rate-limited transcription, a polymerase, once initiated, will travel the length of a gene (e.g., ~3.5 kbp for *hb*) at some effective speed and produce a transcript. The statistics of initiation thus translate directly into the statistics of transcriptional output. Upper: at a given moment, an active transcription site will have a number N of actively transcribing polymerases distributed along its length (red dots), each carrying a partially finished transcript (vertical black lines) that is already capable of binding some of the fluorescent probes. For a particular transcription site, its fluorescent intensity in "cytoplasmic units" measures the total length of all unfinished transcripts in units of length of a complete transcript; this depends on the exact location of all polymerases and bound probes. On average, however, one finds a very simple linear relation: $F = \alpha N$, where α depends only on the location of probe binding sites on the transcript. If probes are homogeneously distributed along the length of the gene, unfinished transcripts form a triangle as shown and $\alpha = 0.5$. For a general arrangement, simple geometric considerations give $0.5 < \alpha < 1$ if the probe distribution is biased toward 5′ end, and $\alpha < 0.5$ when biased toward 3′. Lower: two-state model of transcription. Transcription initiation can occur only if the promoter is in the "Transcription factor (TF) bound" state. The assembly of RNAP complex is treated as a process with a single rate-limiting step k_{RNAP}. In this model, at saturation of input ($k_{ON} * [TF] \gg k_{OFF}$), RNAP loading becomes a single-step process with Poisson statistics. Our results rule out this model, demonstrating that transcription noise is significantly super-Poissonian even at saturated input.

(D) Transcription activity as a function of time in embryos ordered by approximate age based on DAPI staining. Nascent mRNA content, which is low immediately following mitosis, attains a nearly constant level that is maintained for the majority of interphase. Error bars represent SDs.

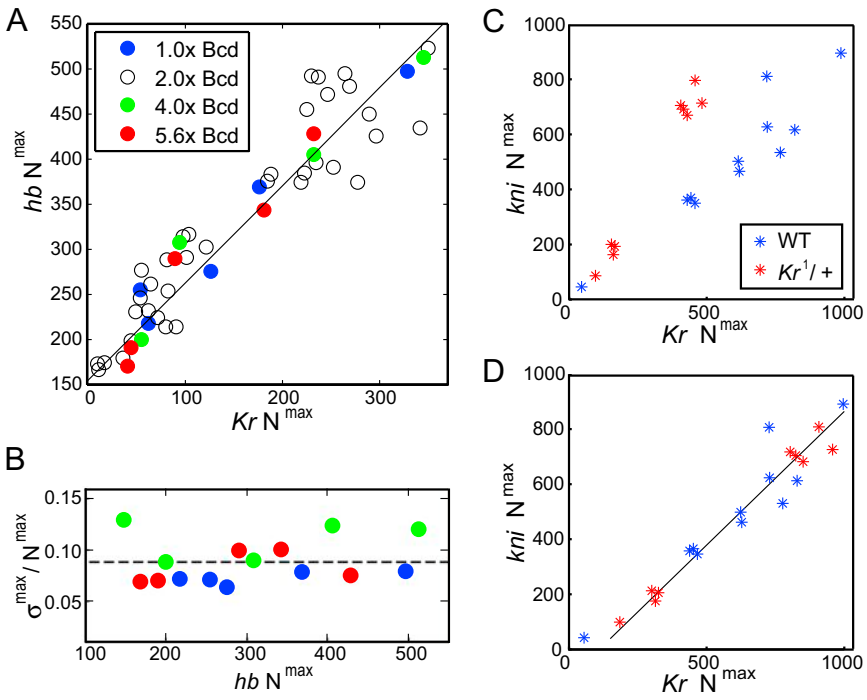

Figure S5. Maximum Gene Expression Rates Are Similar and Independent of Input Genetic Dosage, Related to Figure 5

(A) *hb* and *Kr* mRNA counts per standard volume were determined in the maximal expression region in embryos derived from females carrying 1, 4, or 6 genomic copies of *bcd*. The resulting Bcd protein content (shown in legend; Liu et al., 2013) ranges from 50% of WT (1.0x Bcd, blue) to 280% of WT (5.6x Bcd, red). Data from Figure 6E (circles) shown for comparison. Time points span nc13 and early nc14. Although expression boundaries of *hb* and *Kr* shift along the AP axis as a function of Bcd dosage (data not shown), production rates are unaltered in the domain of highest expression.

(B) Fractional SD σ^{max}/N^{max} within the spatial domain of highest *hb* mRNA accumulation as a function of the mean count for the embryos shown in A. Expression noise across embryos in this experiment is 9% ± 2%.

(C and D) *kni* mRNA expression versus *Kr* mRNA expression in embryos from nuclear cycles 13 and 14. mRNA expression is measured as mean absolute mRNA count per standard volume in the region of maximum expression of the respective gene. As in Figures 6D and 6E, data for WT embryos (blue) coincides with data for embryos deficient in one chromosomal copy of *Kr* (*Kr*^{1}/+; red) if *Kr* concentration in heterozygous embryos is multiplied by 2, demonstrating linearity of the final mRNA output in number of available loci. Raw data shown in (C), rescaled in (D).

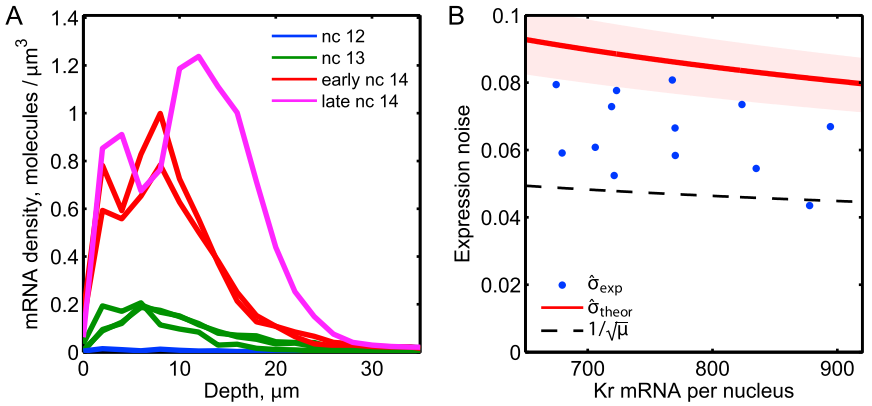

Figure S6. Spatial and Temporal Averaging, Related to Experimental Procedures

(A) *Kr* transcript density as a function of distance from the apical surface (depth). Nuclei inhabit the region surrounding a depth of ~5 μm. Transcripts accumulate several μm basally from nuclei as development proceeds, indicating transcript mobility and the presence of spatial averaging.

(B) For a source with super-Poissonian noise statistics, with a SD σ_{nuc} per N_0 mRNA molecules produced, the maximum efficiency of noise reduction via temporal integration is achieved by a maximally uncorrelated process: independently running the process m times, we find that at mean $\mu = mN_0$ the SD of the accumulated output is given by $\sigma_{nuc}\sqrt{m}$. The predicted relation (red line) between the mean and the observed fractional noise of the mRNA profile is therefore bounded from below by $\hat{\sigma}_{cyto} = \sqrt{\hat{\sigma}^2_{nuc} N_0/\mu + \eta^2}$, where $N_0 = 100 \pm 20$ and $\hat{\sigma}_{nuc} = \sigma_{nuc}/N_0 = 22 \pm 3\%$ are measured directly (nascent mRNA content and its SD, respectively) and a conservative estimate for the measurement noise η is 3% (see Figure S2C). Shaded red area corresponds to uncertainty due to error in parameter estimation. The experimentally observed cytoplasmic expression noise as a function of *Kr* accumulation (blue points) shows that mRNA profiles exhibit better precision, suggesting the presence of spatial averaging. Poisson (counting noise; $1/\sqrt{\mu}$) fluctuations are shown for comparison (dashed line).